Assessment of infragravity waves

Theme: Hydrodynamic Modelling
WAMSI Westport Marine Science Program

WESTERN AUSTRALIAN MARINE SCIENCE INSTITUTION

WESTPORT

Better science **Better decisions**

WAMSI WESTPORT MARINE SCIENCE PROGRAM

WESTERN AUSTRALIAN MARINE SCIENCE INSTITUTION

WESTPORT

ABOUT THE MARINE SCIENCE PROGRAM

The WAMSI Westport Marine Science Program (WWMSP) is a $13.5 million body of marine research funded by the WA Government. The aims of the WWMSP are to increase knowledge of Cockburn Sound in areas that will inform the environmental impact assessment of the proposed Westport development and help to manage this important and heavily used marine area into the future. Westport is the State Government's program to move container trade from Fremantle to Kwinana, and includes a new container port and associated freight, road and rail, and logistics. The WWMSP comprises more than 30 research projects in the biological, physical and social sciences that are focused on the Cockburn Sound area. They are being delivered by more than 100 scientists from the WAMSI partnership and other organisations.

FUNDING SOURCES
The $13.5 million WAMSI Westport Marine Science Program was funded by the Western Australian Government, Department of Transport. WAMSI partners provided significant in-kind funding to the program to increase the value to >$22 million.

DATA
Finalised datasets will be released as open data, and data and/or metadata will be discoverable through Data WA and the Shared Land Information Platform (SLIP).

YEAR OF PUBLICATION
January 2025

This report is for the project: Surface gravity wave modelling.

CITATION
Pattiaratchi, C. (2025). Assessment of infragravity waves. Prepared for the WAMSI Westport Marine Science Program. Western Australian Marine Science Institution, Perth, Western Australia. 42 pp.

FRONT COVER IMAGE
Theme: Hydrodynamic modelling
Front cover image: Ocean wave (pexels.com).

Contents

The WAMSI Westport Marine Science Program is a $13.5 million body of research that is designed to fill knowledge gaps relating to the Cockburn Sound region. It was developed with the objectives of improving the capacity to avoid, mitigate and offset environmental impacts of the proposed Westport container port development and increase the WA Government's ability to manage other pressures acting on Cockburn Sound into the future. Funding for the program has been provided by Westport (through the Department of Transport) and the science projects are being delivered by the Western Australian Marine Science Institution.

1 Assessment of infragravity waves

Author/s
C Pattiaratchi, The University of Western Australia

Project
5.2 - Surface gravity wave modelling

Executive Summary

Surface gravity waves incident on a coastal region can be classified into three main groups depending on their period: (1) sea waves, generated by local weather, with periods between 2 and 8 s; (2) swell waves, generated by distant storms, with periods between 8 and 25s; and, (3) infragravity waves, with periods between 30 and 300 s. Infragravity waves due to the formation of wave groups, or "sets." When wind-waves of similar periods travel together, they group, resulting in varying wave heights within the groups. This wave height variation at the group scale forces ocean surface infragravity waves. Coastal circulation, flooding, sand transport, and erosion are strongly influenced by these infragravity waves, especially during storm events. They also have a large influence on forcing oscillations in marinas and ports that influence vessel motion. The aim of this project was to complete an assessment of infragravity period wave activity in Cockburn Sound, particularly along the Stirling Channel, using existing field measurements. In this report, we define 'infragravity waves' or IG waves as those with periods between 30 s and 200 s that are important for vessel movements.

We analysed a unique data set that included continuous sampling of water levels at 2 Hz intervals from three locations and two separate years: Stirling Channel (2020, 2022), Parmelia and Success (Figure 13). The data were analysed using a dedicated MATLAB toolbox OCEANLYZ (Karimpour and Chen, 2017) in the frequency domain.

The main outcomes of the study are as following:

(1) Water level spectra at each of the location and throughout the year did not indicate specific periods in the 30-200 s band, rather the spectral energy was distributed almost uniformly across the IG periods. There were no peaks higher than the 95% confidence interval.
(2) The time-frequency water level spectra indicated increased energy in the 30-200 s band when the incoming swell was > 15 s. This is typical for this region of the coast.
(3) In the Stirling Channel, the infragravity significant wave height (H_{IG}) was generally low with maximum values of 0.10 m, achieved during storm events.
(4) There was no clear relationship between significant wave height (H_s) and infragravity significant wave height (H_{IG}), although in general, higher H_{IG} was associated with higher H_s.

It is concluded that the infragravity wave activity is relatively low in Cockburn Sound and in particular in the Stirling Channel. Higher H_{IG} was mainly associated with storm systems, particularly during winter when the incoming swell period was > 15 s.

2 Introduction

Ocean surface gravity waves usually follow a Rayleigh distribution in terms of both wave height and period. They have different disturbing forces for generation and restoring forces for propagation (Figure 1). Energy in most ocean waves originate from the generating force made by wind blowing over the ocean surface, and they propagate across the ocean due to the restoring force of gravity. A major part of the energy is accumulated under the broad-banded (1-30 s) gravity waves (or wind waves), while very sharp and narrow-banded (12 hr and 24 hr) tidal waves also contribute for relatively high energies (Kinsman, 1965; Giese and Chapman, 1993). Waves in between the above two wave bands have periods in the range of 30-300 s and have relatively low energy (Figure 1). They are generally known as a part of long waves, however, after Kinsman (1965), they are specifically named as 'infragravity waves'.

Surface gravity waves incident on a coastal region can be classified into three main groups depending on their period: (1) sea waves, generated by local weather, with periods between 2 and 8 s; (2) swell waves, generated by distant storms, with periods between 8 and 25 s; and, (3) infragravity waves, with periods between 30 and 300 s.

The aim of this project was to complete an assessment of infragravity period wave activity in Cockburn Sound, particularly along the Stirling Channel, using existing field measurements. In this report, we define 'infragravity waves' or IG waves as those with periods between 30 s and 200 s that are important for vessel movements.

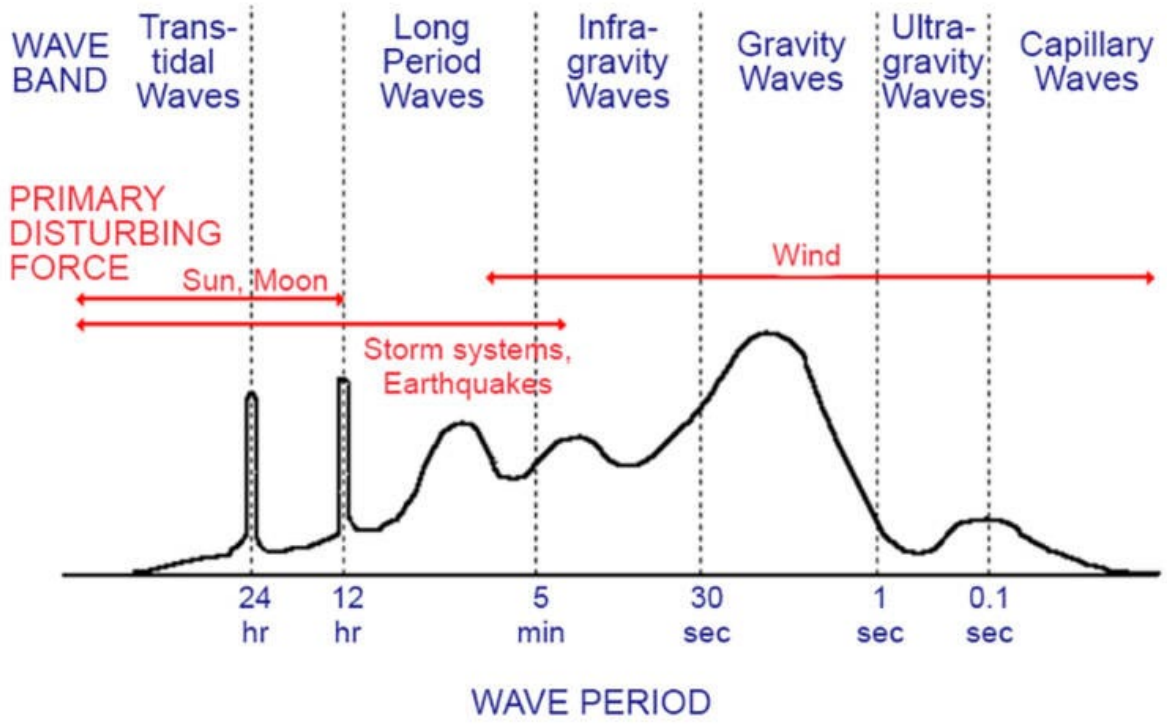

Figure 1. Schematic representation of the energy contained in the surface waves of the ocean and definitions based on periods of the different waves (modified from Kinsman, 1965).

2.1 Generation and classification of infragravity waves

Infragravity waves are generated through nonlinear interactions among wind or swell waves, by transferring energy from high frequency waves to low frequency waves (Gallagher, 1971). It has been found that they dominate the near shore velocity field (Bowen and Huntley, 1984) and hence, can be very energetic close to shore (Herbers et al., 1994; 1995b).

The classification of infragravity waves is mainly based on their generation mechanisms. Some of these generation mechanisms of infragravity waves are schematically illustrated in Figure 2. In this study, we are not particularly interested in the shallow surf zone but rather in the coastal zone (e.g. Kwinana shelf) where the water depths are ~10 m.

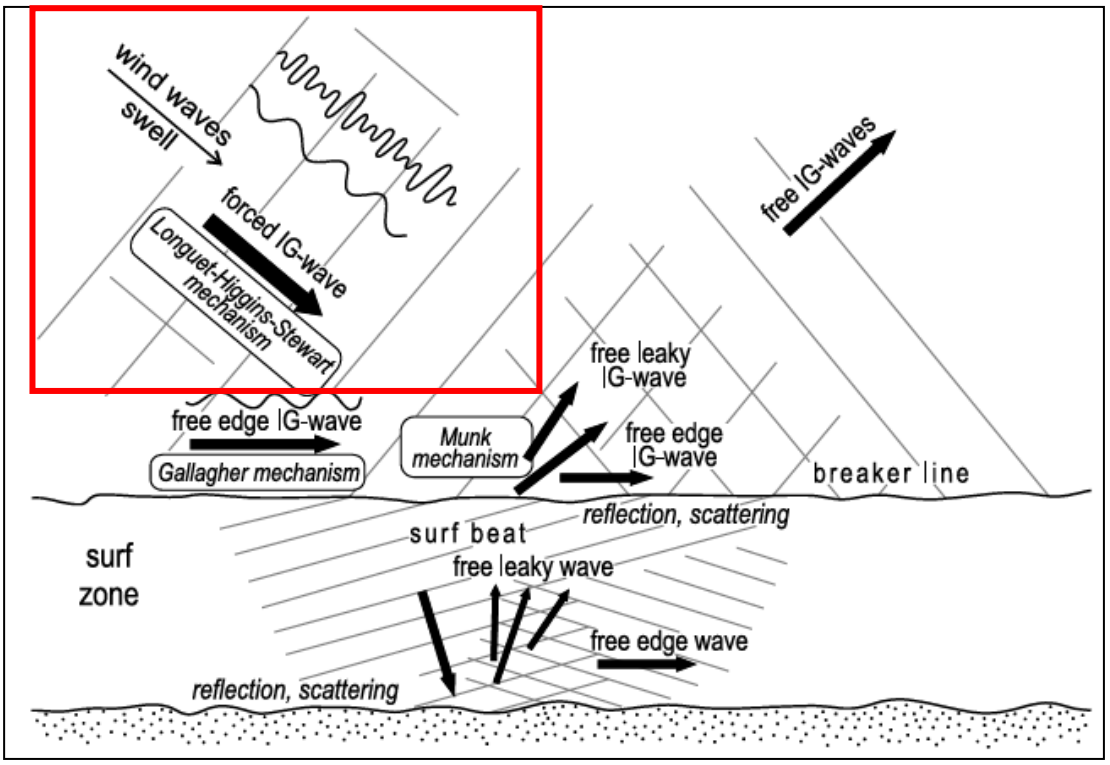

Figure 2. Generation mechanisms of infragravity waves in the coastal zone (Rabinovich, 2009). The processes relevant to this study are shown within the red box.

2.1.1 Bound infragravity waves

Swell waves propagating towards shore tend to travel as well-defined sets of waves with narrow frequency bands called 'wave groups' (popularly called wave sets). A wave group is a finite series of individual waves with a wave front and a wave end propagating in the same direction in a random wave field with the group velocity (Van Rijn, 1990). The addition of two waves with slightly different periods generate modulation of the signal to create wave groups (Figure 3). One effect of wave grouping is to create set-down beneath wave groups (Figure 3b). The mechanism producing set-downs begins with the variation of the water particle velocity, which is higher in groups of high waves and smaller in between the groups. This results in a decrease of the water pressure beneath groups of high waves compared with the pressure in between the groups. Consequently under a constant air pressure, , the mean sea level is depressed beneath the high wave groups and corresponding rise in the mean sea level occurs in between the groups in low wave heights (Bowers, 1977), as shown in Figures 3 and 4. This variation in mean sea levels induces a wavelike flow called 'bound' long waves or bound infragravity waves, as they are locked to the wave group. This mechanism can also be explained

in terms of radiation stress gradient changes in high and low wave groups as shown by Longuet-Higgins (1964). The generated bound infragravity wave is 180° out of phase with the incident wave group (Figure 3b). It has the same periodicity and the same lengths as the wave group and travels with the group velocity of swell waves, which is significantly smaller than the phase velocity of waves with the same frequencies (Rabinovich, 2009).

When there is an incoming swell, Munk (1949) and Tucker (1950) first noticed the existence of longer waves, of 2-3 min period, similar to the envelope of the visual swell, and suggested that the long waves may be caused by an excess of mass transported forward by groups of high swell. Longuet-Higgins and Stewart (1964) explained the formation of these long waves as a wave group, containing larger than average waves, would depress the mean water surface and thereby forces a long wave which was defined as a group bound long wave. Longuet-Higgins and Stewart (1964) theoretically demonstrated the formation of group bound long wave using the gradient in radiation stress as a wave group passes. Therefore, wave groups are always associated with a group bound long wave (Figure 1). Several investigators (Elgar et al. 1992; Herbers et al. 1995) have demonstrated that bound long wave energy increases with an increase in swell energy and a decrease in water depth. Bound waves are usually more significant when energetic swell conditions exist.

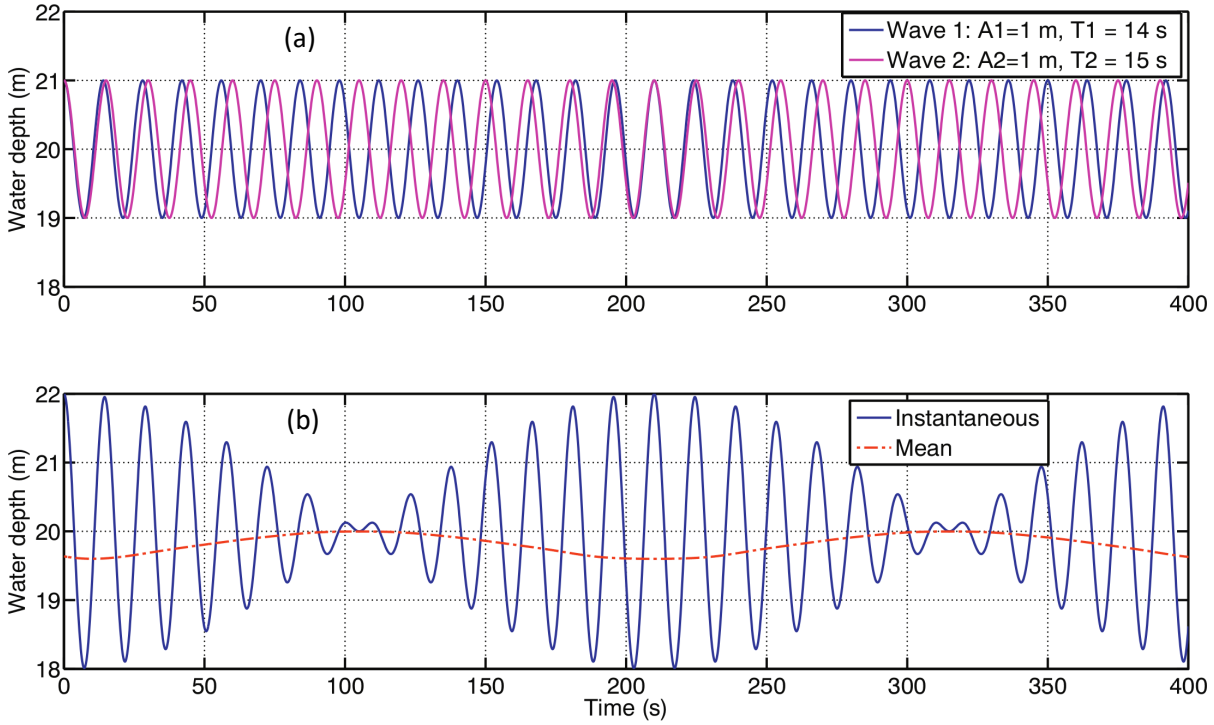

Figure 3. (a) Time series of two sinusoidal waves traveling over a flat bottom by 20 m water depth with same wave height but different periods; (b) Resulting free surface elevation (blue) and bound wave (red) from Bertin et al. (2018b).

2.1.2 Free infragravity waves

Tucker (1950) observed that offshore records of wave pressure on the seabed often show an existence of longer waves of 2-3 minutes periods, in the presence of swell waves. He suggested that these long waves may be caused by the mass-transport associated with the breaking of high swell wave groups (Longuet-Higgins, 1962). As a wave group reaches the breaker zone, the bound long waves locked to the wave group are released from the group as free long waves (or free infragravity waves), radiating one elevation in shoreward and another in seaward, leaving a depression in between. The shoreward elevations, having reflected at the beach before propagating out to sea again, establish a sequence of

elevations and depressions (Tucker, 1950). It creates a field of standing waves consisting of free long waves. The mechanism of creating these consecutive elevations and depressions in mean sea level was first observed by Munk and he called it 'surf beats' (Tucker, 1950).

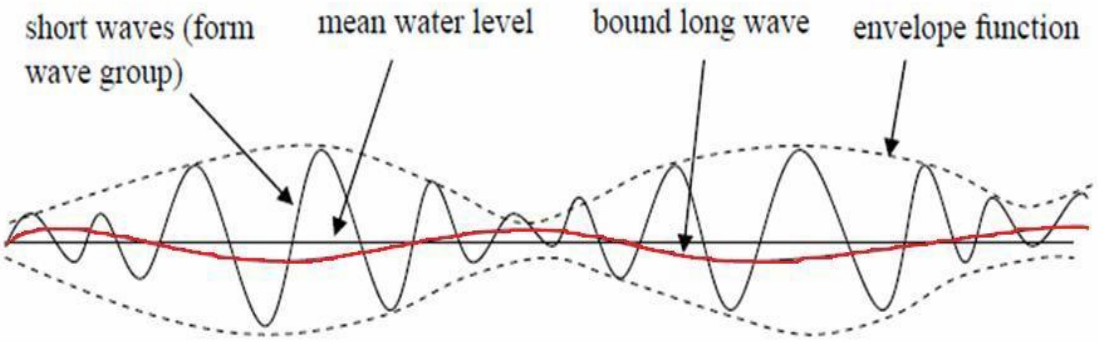

Figure 4. Profile of bound long wave, shown in red (Kularatne and Pattiaratchi, 2008)

2.1.3 Free leaky and edge infragravity waves

After reflection at the shoreline, the released free long waves propagate in a seaward direction and may radiate into deep ocean as free leaky waves or remain refractivity trapped to the shore as edge waves (Huntley, 1976; List, 1992; Herbers et al., 1995b; Ruessink, 1998). Free edge waves have a spatial variation of amplitude which is sinusoidal along the shore and exponentially decaying in the offshore direction (Huntley, 1976).

There are a number of observations of wave conditions near the shore that suggest both free leaky waves and free edge waves are important components of this infragravity frequency motion (Huntley, 1976; Bowen and Huntley, 1984; Elgar et al., 1992), especially the free edge waves which contribute a significant proportion of the total energy of the low-frequency motion (Huntley, 1981; Bowen and Huntley, 1984; Okihiro et al., 1992; Ruessink, 1998). Gallagher (1971) demonstrated that under certain conditions, these free edge waves can be excited by the incident wave groups. This mechanism was further discussed by Bowen and Guza (1978) who concluded from laboratory evidence that surf beats are predominantly a free edge wave phenomenon (Holman, 1981).

2.1.4 Free infragravity waves over uneven topography

Liu (1989) showed that free infragravity waves can be generated by the refraction of wave groups propagating over uneven topography. Several later studies also identified the generation of free infragravity waves by: breaking of wave groups (Nakamura and Katoh, 1993); refraction of short wave groups over an uneven topography (Janssen et al., 2003; Thomson, 2006; Zou, 2011); and, refraction of short wave groups over a shallow reef (Péquignet et al., 2009; Nwogu and Demirbilek, 2010). Fringing coral reefs and rock platforms have been documented to be effective in generating infragravity waves (Péquignet et al., 2009; Beetham and Kench, 2011). In a study of wave behaviour in a fringing coral reef, Nwogu and Demirbilek (2010) found that the majority of the wave energy in the incident wave frequency band was dissipated within a few wavelengths of the reef face, and the infragravity wave energy increased as the waves moved over the reef flat. Similarly, McComb et al. (2009) found that offshore of Geraldton, majority of the infragravity wave energy was generated during swell wave transformations over a 3 km wide reef platform located offshore. These studies indicate that in regions of complex topography, such as those with offshore reef systems, there is a local source of infragravity wave energy generation.

2.1.5 Summary: infragravity waves

From the above sections we can develop a summary of infragravity waves:

- Defined as wave energy contained in periods of 30 s to 200 s.
- Wave lengths from 100 m to 10 km.
- Generated through the nonlinear interaction of wind waves.
- Often associated with wave groups ('sets') formed by interference between two or more wave trains of different periods, moving in the same direction.
- Travel with the group velocity, which is significantly smaller than the phase speed of free long waves with similar frequencies.
- Defined as infragravity waves (proposed by Kinsman, 1965).

2.2 Infragravity gravity wave climate in Western Australia

Western Australia is subject to swell that is generated very far away. For example, waves generated in the South Atlantic Ocean off Brazil propagate through vast oceans before having an impact in Western Australia. These waves take more than 15 days to travel and only the longer period waves make the journey. Wave celerity (wave speed) is related to wave period and as the waves propagate long distances, they order themselves according to wave period – this is called the dispersive effect of the waves. Thus, waves trains that travel over long distances have wave periods clustered together which are conducive wave grouping (Figures 3 and 4) with energy in the infragravity wave band.

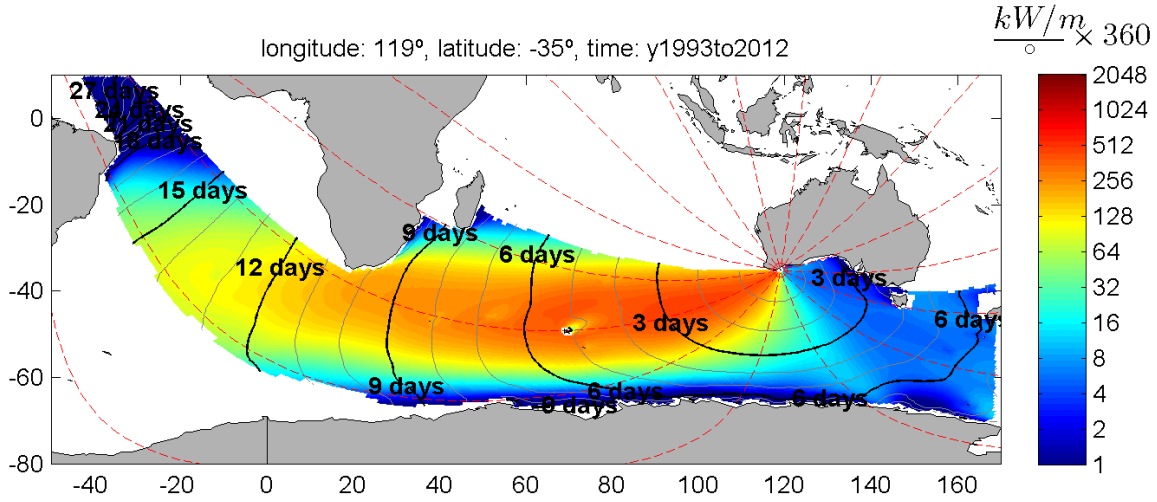

Figure 5. Deep water wave energy propagation to Western Australia.

Globally, the southern Indian Ocean, due to the influence of the Southern Ocean storms and the relatively shorter extent of the African continent to the south, results in higher infragravity wave heights, although the maxima are 0.04 m (Figure 6). As expected, there is a significant seasonal variation in IG wave heights with higher values during the austral winter months (Figure 6b).

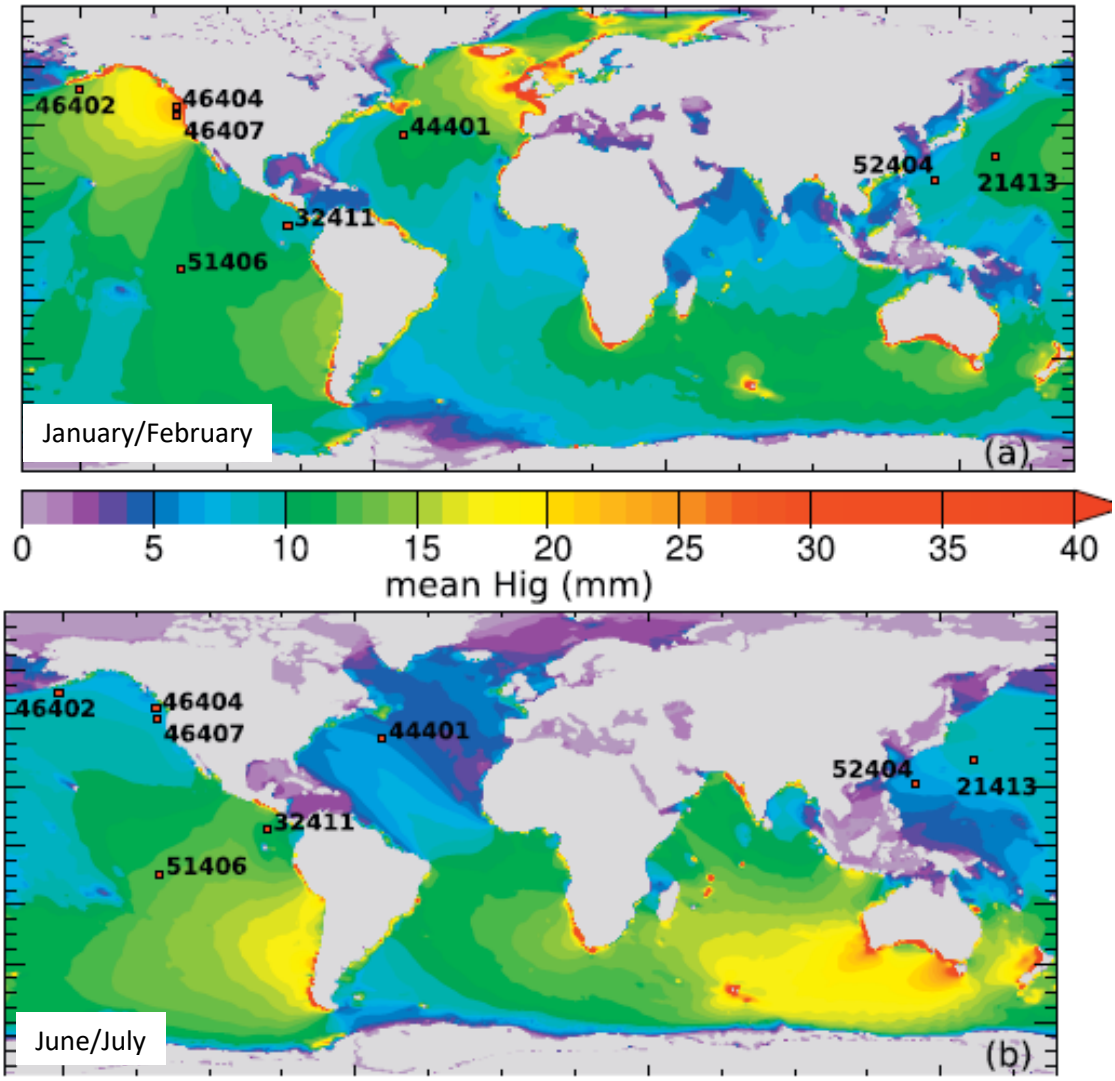

Figure 6. Mean values of infragravity wave height (Hig): (a) January and February; 2008 and, (b) June and July 2008. Note maximum wave heights are 4 cm. From Ardhuin et al. (2014).

Typical water level spectra, based on 2-3 months of continuous underwater pressure measurements at locations in south-west Australia, show the dominant periods contained in the water level records (Figure 7). In the longer periods, there are energy peaks at 24 and 12 hours that are related to tidal forcing and another peak at ~2 hours which is the continental shelf seiche, a common feature in the study region. This period is dependent on the width of the continental shelf and therefore changes depending on location. The Jurien Bay record obtained at 10 m water depth highlight the typical open ocean incident wave energy. The major peak in the higher frequencies is at 15 s, associated with the incident swell waves (Figure 7a). There are no specific energy peaks in the infragravity band 30-300 s but there is a linear decrease in IG energy from ~40 to 300 s. In contrast, at Cowaramup, also at 10 m water depth but immediately offshore of Cowaramup Bay indicates a strong peak in IG energy at ~100 s which is related to the oscillations in the Bay (Figure 7b). The two stations which have closed basins are: Two Rocks Marina (Figure 7c) and Geraldton Port (Figure 7d). Both have several energy peaks in the IG bands which are directly related to the different modes of oscillations inside the basins (Thotagamuwage and Pattiaratchi, 2014).

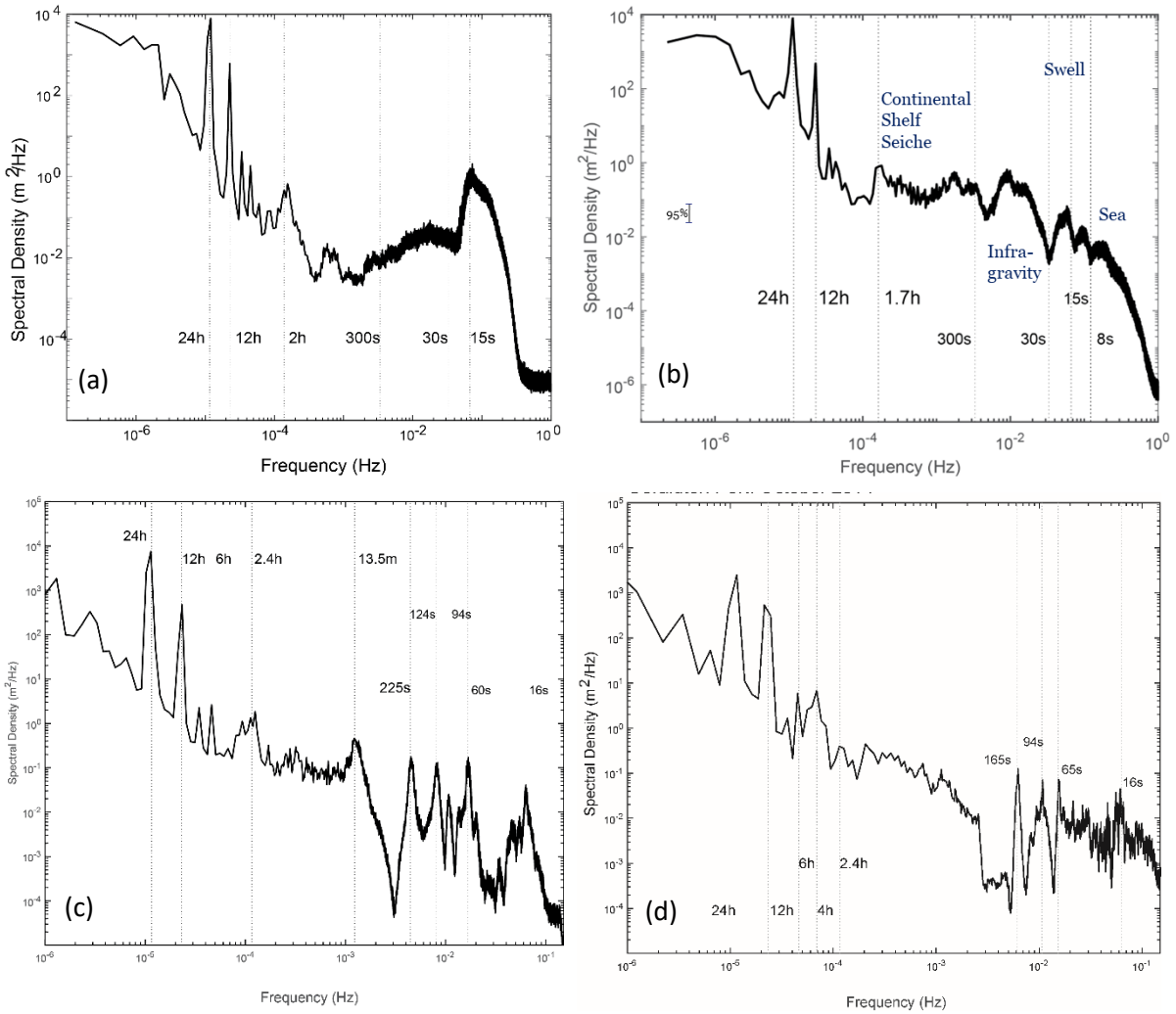

Figure 7. Typical sea level spectra from the west Australian coast: (a) Off Jurien Bay in ~10 m water depth; (b) Cowaramup Bay; (c) Two Rocks marina; and, (d) Geraldton Port.

Time-frequency water level spectra provide the time variability of the spectral energy in the waves. This contrasts with obtaining water level spectra for the complete record of 2-3 months as shown in Figure 7. Wave celerity in deep water is directly proportional to wave period. Hence, waves with higher wave periods travel faster. When waves are generated from a distant storm, the longer period waves arrive at the shoreline first and there is a gradual decrease in wave period with time. This is reflected in the time-frequency water level spectra (Figure 8). An example for Jurien Bay shows four storms with initial wave periods > 15 s and gradually decreasing in period (as shown by blue dashed lines; Figure 8). The best example of these is a storm that started on 25 December 2016 and the longest wave period resulted in higher IG energy (Figure 8). For these four storms, there is increased energy in the IG band (30-300 s). The red dashed lines represent locally generated waves due to sea breeze.

This pattern can be seen more clearly in a three-dimensional plot of time-frequency water level spectra from Jurien Bay that separates the different peaks at 8 s (sea waves), 15 s (swell waves), 30-300 s (IG waves) and the continental shelf seiche (Figure 9).

Extending the time-frequency water level spectra for Jurien Bay, Cowaramup Bay and Two Rocks marina show the time variability of the IG energy at each location (Figure 10). At all three locations (also at most locations along the west coast of WA), there are specific periods when high IG waves are present, and they generally correspond to when the incident swell waves have periods > 15 s. This is clear at Jurien Bay (in 10 m water depth) where there were ~15 events (over a two-month period) with

incident swell periods > 15 s that were also associated with higher spectral energy in the 30-300 s IG band (Figure 10a). A similar pattern was present in Cowaramup Bay (~10 storms) with more pronounced locally generated waves with periods < 8 s (Figure 10b). At Two Rocks Marina, there is a different pattern due to the enclosed nature of the marina. The natural period of oscillations inside the marina at 60, 124 and 225 s were present almost continuously (Thotagamuwage and Pattiaratchi, 2014) but was enhanced when the incident swell periods are > 15 s (Figure 10c).

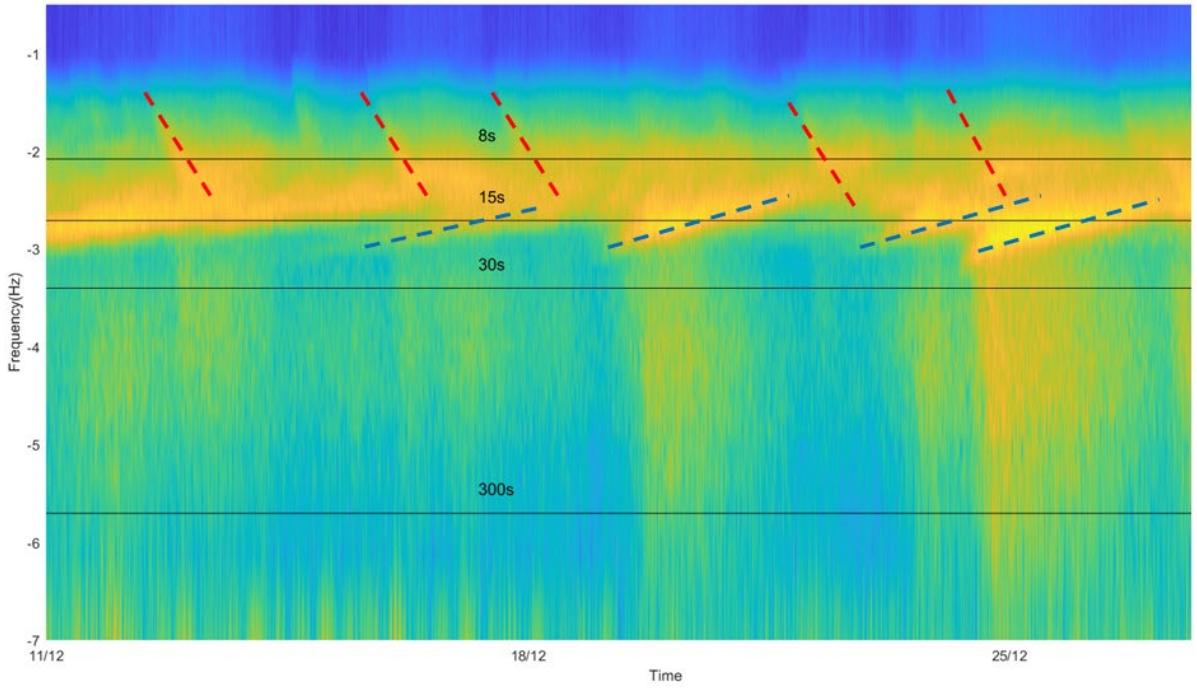

Figure 8. Example time-frequency sea level spectra from the west Australian coast showing the relationships between storms and IG energy. Blue dashed lines indicate swell waves whilst red dashed lines reflect locally generated waves (sea breeze).

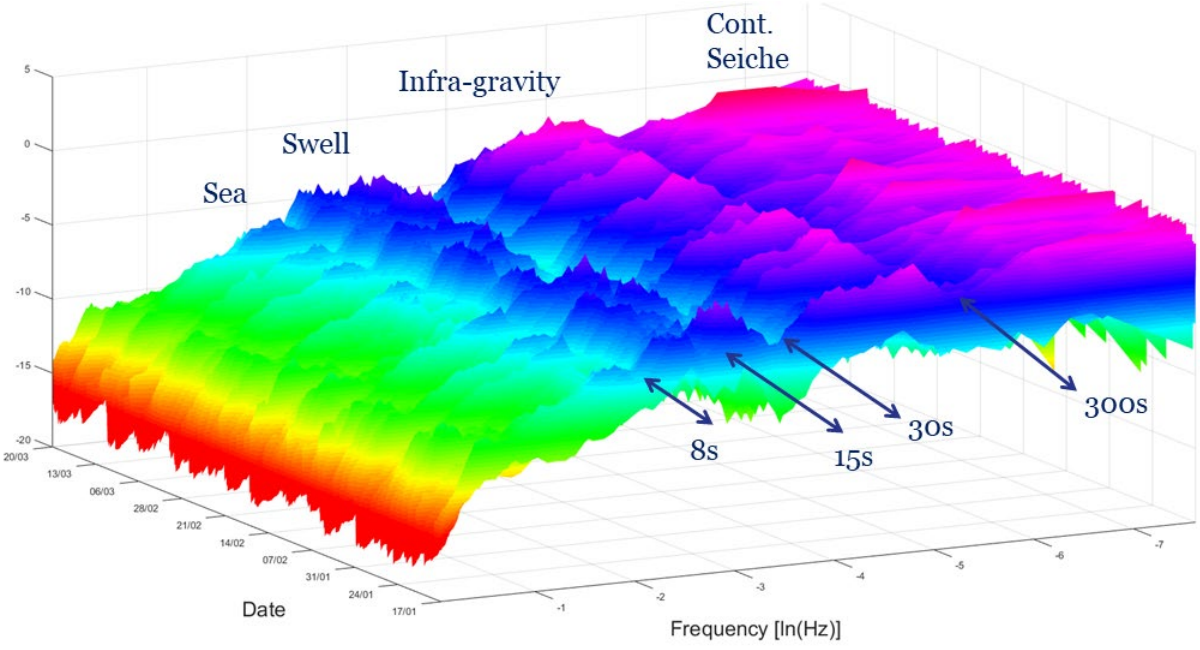

Figure 9. Time-frequency sea level spectra from the west Australian coast showing the bands of different periods and physical phenomena. The vertical axis is normalized relative spectral energy.

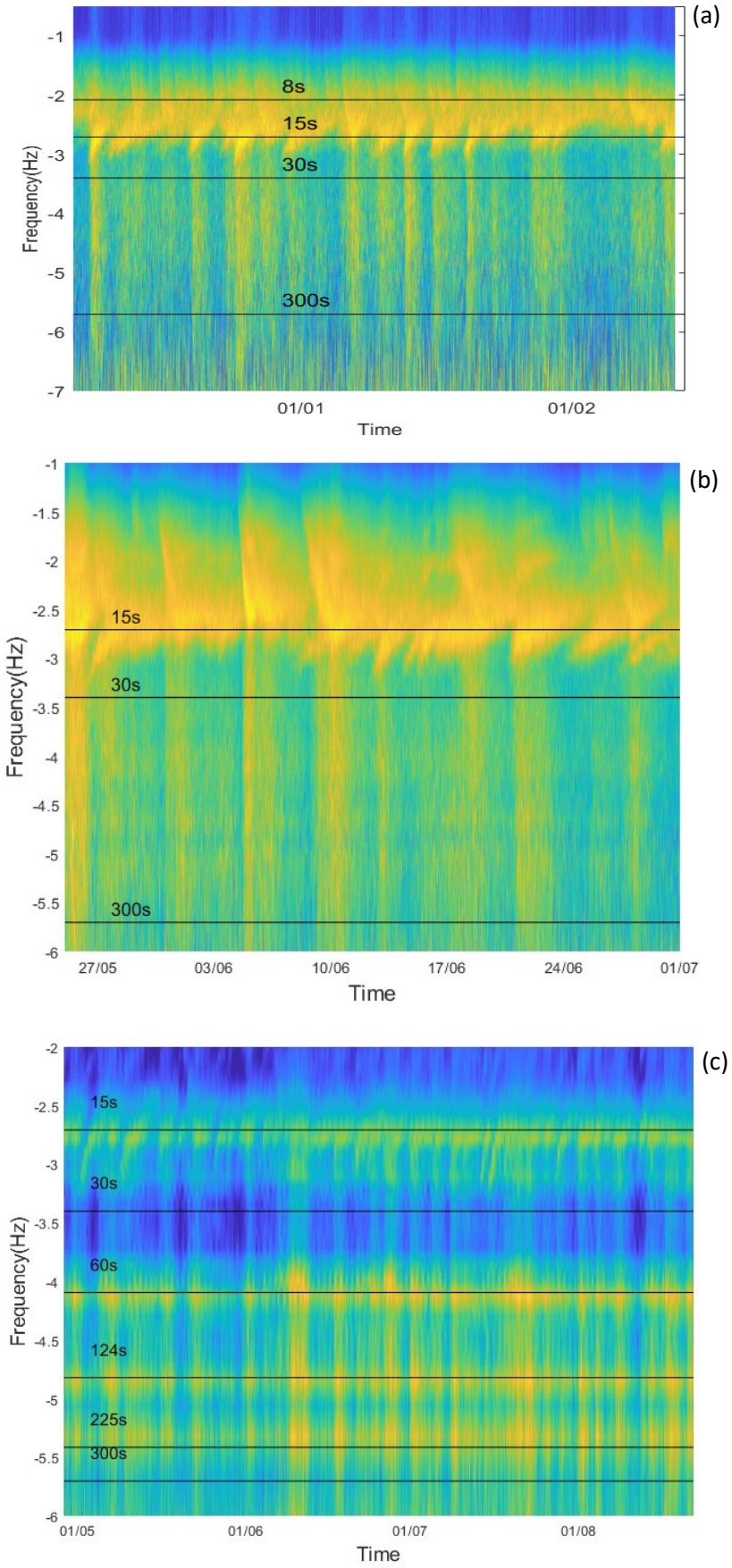

Figure 10. Time-frequency sea level spectra from the west Australian coast: (a) Off Jurien Bay in ~10m water depth; (b) Cowaramup Bay; (c) Two Rocks marina.

Scatter plots of significant swell wave height and IG wave heights demonstrate an almost linear relationship (Figure 11), particularly for lower swell heights. In general, at Jurien Bay, the maximum swell and IG wave heights were 3.5 and 0.9 m, respectively, with the slope of the best fitting line indicating that the IG waves were ~10% of the significant swell wave height (Figure 11a). For Geographe Bay, the maximum swell and IG wave heights were 1.9 and 0.17 m, respectively, with the slope of the best fitting line indicating that the IG waves were ~7% of the significant swell wave height (Figure 11b).

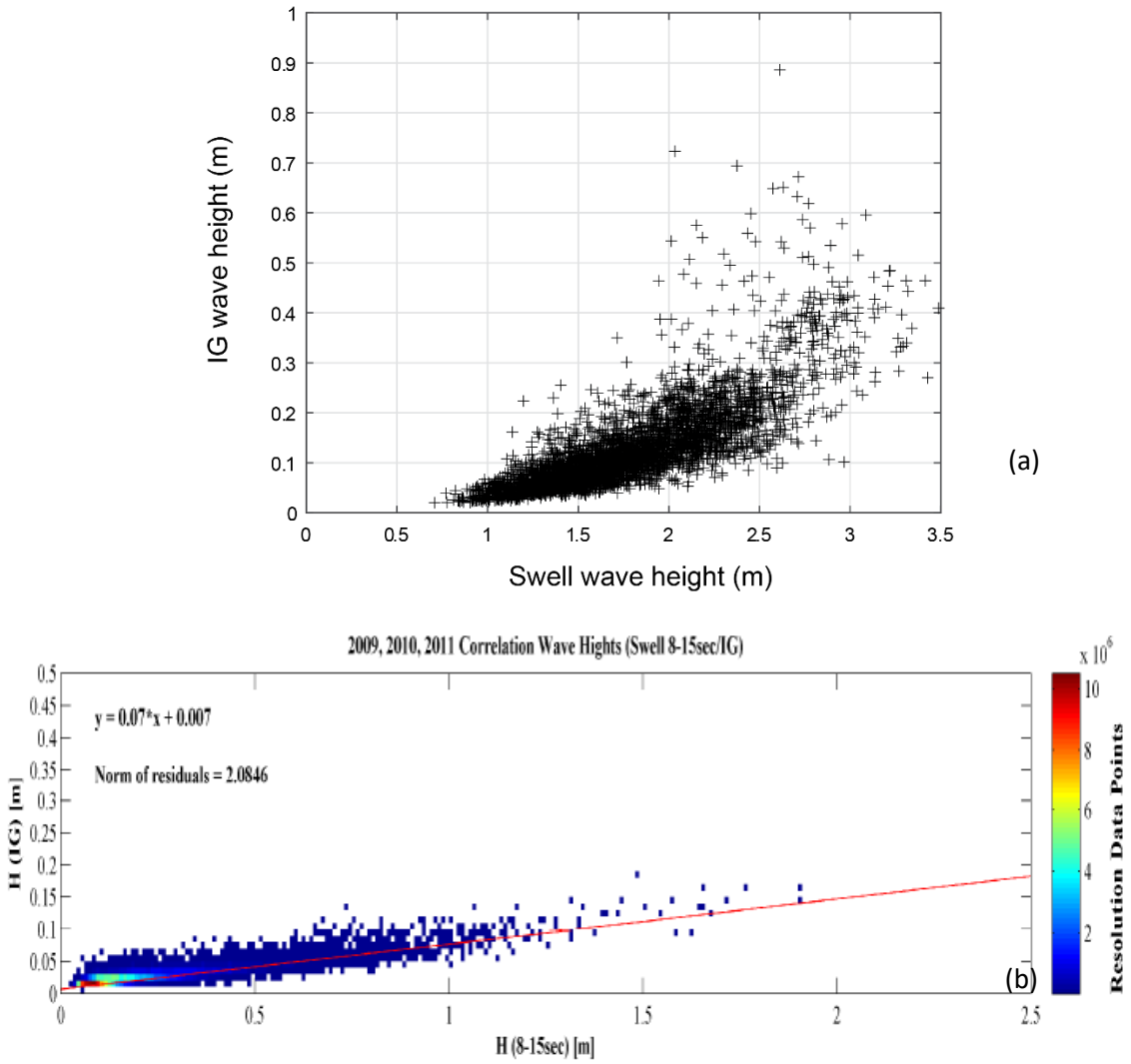

Figure 11. Scatterplots of significant wave height and IG wave height: (a) Off Jurien Bay in ~10 m water depth; (b) Geographe Bay.

Cockburn Sound is an enclosed basin with only the opening between Garden and Carnac Islands allowing waves to penetrate the Sound (Figure 12). The northern boundary of the Sound is shallow which causes most of the waves to break (Parmelia and Success Banks) and, thus, minimal IG waves penetrate the Sound. As the IG waves are a combination of the incident swell waves, it is expected that, in deeper water, the IG wave directions will be similar to the swell wave directions. When the waves approach the coastline, many processes contribute to the generation of IG waves nearshore as shown in Figure 2. Therefore, for southern Kwinana shelf, the IG wave directions are most likely to be from the north-west quadrant.

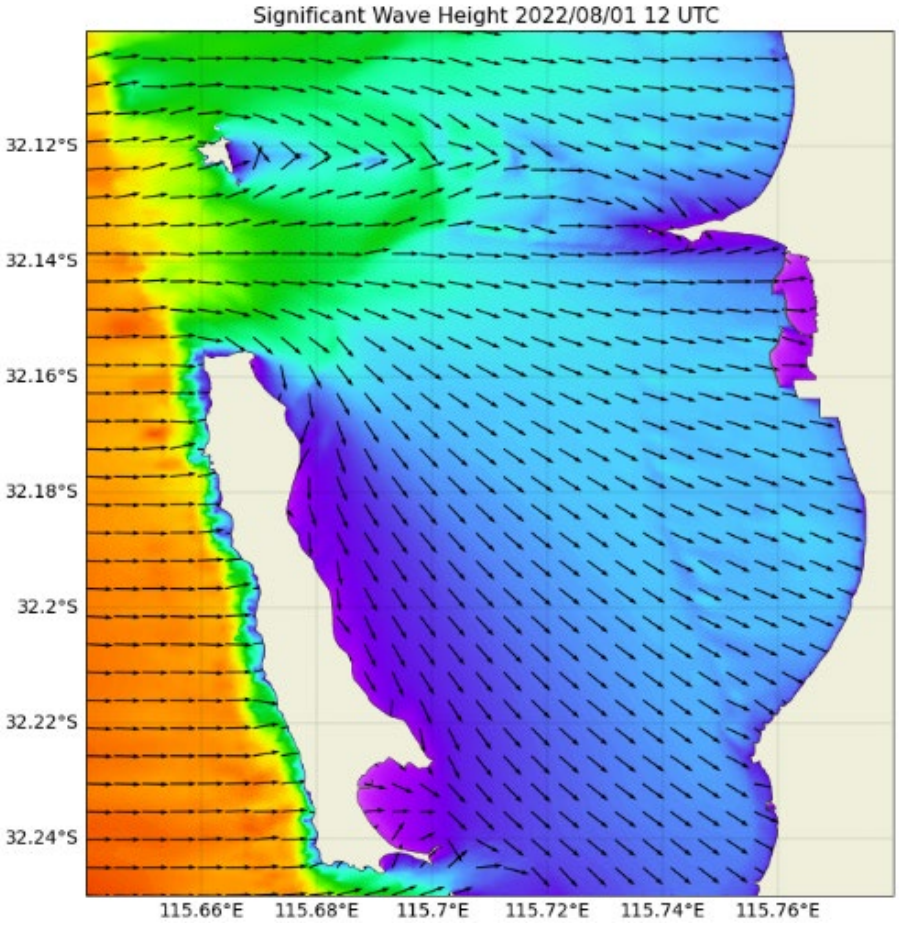

Figure 12. Predicted incident wave directions in Cockburn Sound during a storm on 1 August 2022. The waves approach the Sound between Garden and Carnac Islands and propagate across the Sound from a north-westerly direction.

3 Materials and Methods

The global definition of infragravity waves is those with periods between 30 and 300 s (Figure 1). In Cockburn Sound the energy in the 200-300s band was relatively low and therefore in this report we adopted that infragravity waves to be in the period 30 s to 200 s which is important for vessel movements.

3.1 Field data

Field data were provided by Fremantle Ports from three locations within Cockburn Sound: Success, Parmelia and Stirling Channel (Figure 13). The data were collected as part of the Fremantle Ports operational metocean monitoring program. Data from 2020-2022 were provided but there were many errors and datum shifts and, therefore, only a section of the data were extracted for analysis and included data from 2020 and 2022 (Table 1). Data from 2021 could not be analysed. The data collected in 2022 covered the whole year, whilst in 2020, the data included the period from 1 May to 30 December 2020 (Table 1).

At all three locations, data were collected using Digiquartz 8CDP pressure sensors that measured the total pressure (seawater and atmospheric) continuously at a sampling rate of 2 Hz (Figure 14). Each pressure sensor was in ~2 m below the mean sea level.

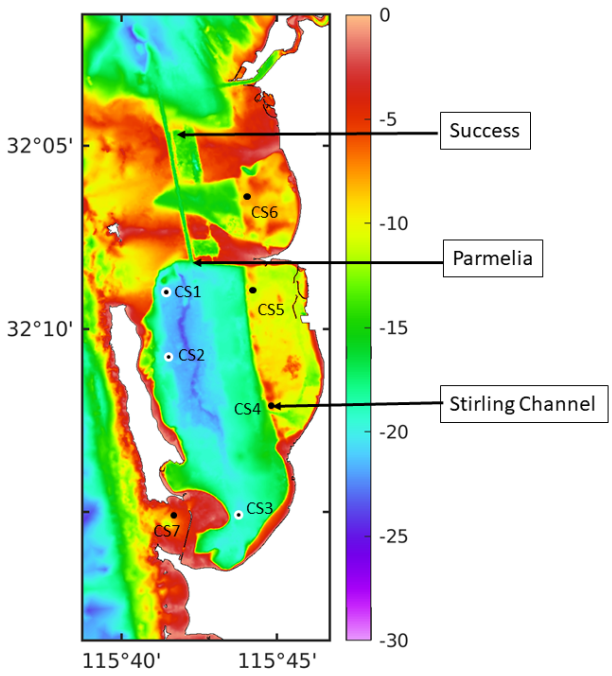

Figure 13. Location of pressure sensor data used in this study: Success, Parmelia and Stirling Channel.

Table 1. Coverage of data analysed as part of this study.

Site	Year	Start	End
Stirling Channel	2022	1 January	31 December
Stirling Channel	2020	1 May	31 December
Success	2020	1 May	31 December
Parmelia	2022	1 January	31 December

Time series data, collected at a 2 Hz sampling interval, includes changes in water levels but is dominated by tides and storm systems (Figure 14). It also shows the seasonal variations in tides and more specifically storm systems. In January 2022, in the absence of storms, the water levels recorded were dominated by diurnal tidal variations (Figure 14a). In May 2022, a couple of winter storm systems were recorded (Figure 14b) whilst in August 2022, many storms were recorded. The storm at the beginning of August 2022 was the biggest storm that was recorded in the Perth region over the past 10 years (Figure 14c). By November, the return to the summer pattern is evident (Figure 14d).

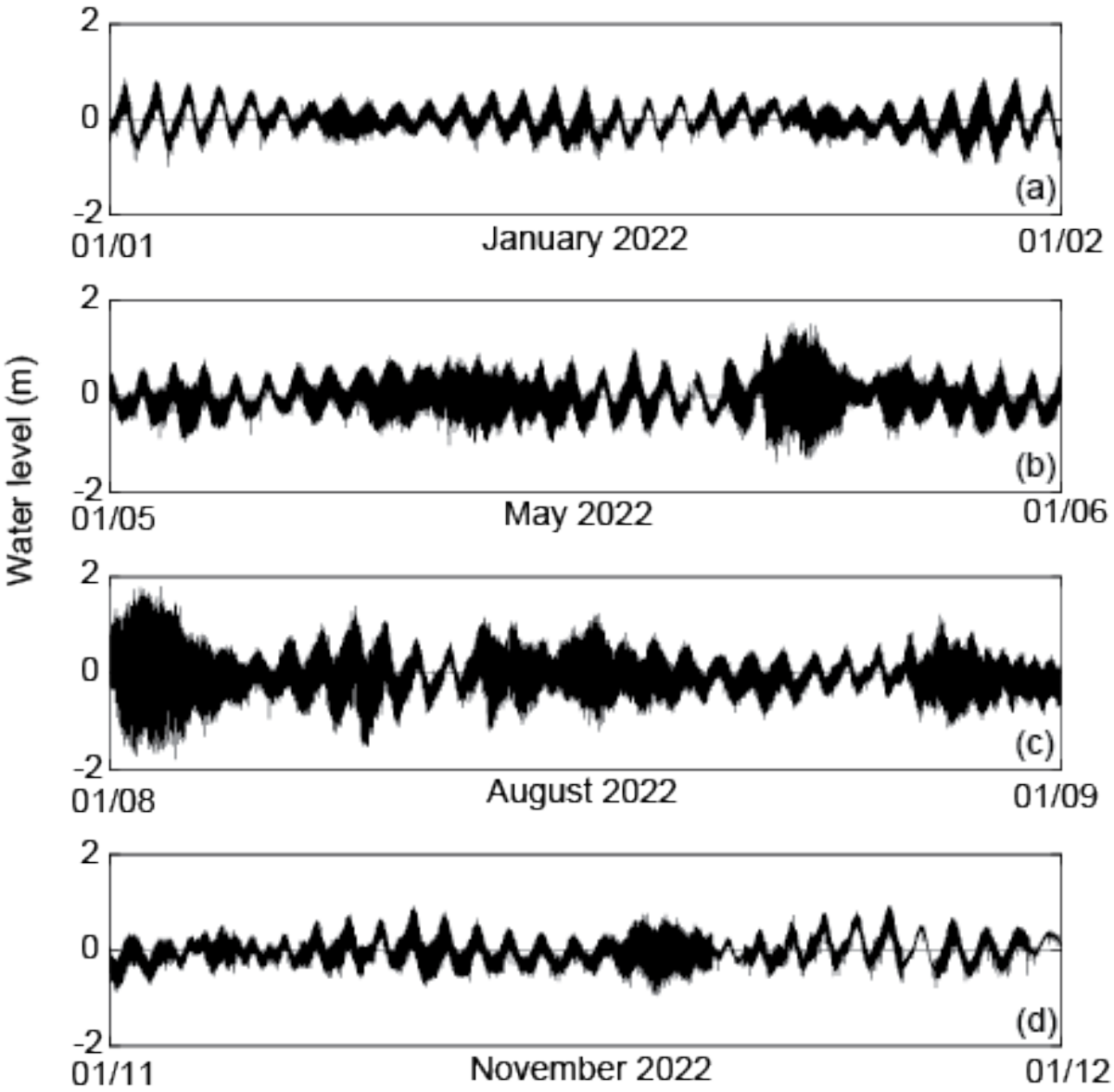

Figure 14. Time series of water level data collected at 2Hz from Stirling Channel in 2022. (a) January; (b) May; (c) August; and, (c) November

3.2 Data analysis

The total pressure data analysed in this study (Figure 13 and Table 1) were recorded continuously as a time series with a sampling interval of 2 Hz. The wave parameters were calculated directly from the recorded time series through transformation of the temporal signal into the frequency domain using Fourier transforms. The analysis was undertaken through separating the time series into hourly bursts (i.e. 7200 data points).

Pressure transducers are common instruments used for wave measurements in coastal regions as they are relatively lower in cost, simple to operate, and with an acceptable level of accuracy. However, it can cause changes in wave data as the pressure signal is attenuated with depth. The data recorded with a pressure transducer contain two sets of signals: (1) a hydrostatic pressure signal, which represents the sensor's depth and is used to define the water depth; (2) a dynamic pressure signal, which is a measure of wave motions, i.e. water surface fluctuations, and is used to estimate wave properties. However, the dynamic pressure resulting from the water surface fluctuations begins to attenuate in the water column as the depth increases from the water surface towards the seabed. As a result, dynamic pressure signals recorded by a pressure sensor are weaker compared to the original values at the water surface. The deeper the pressure sensor is located, the higher the pressure signal has to attenuate. Therefore, the dynamic pressure signal from a pressure transducer cannot be directly used for wave analysis, and requires correction and processing prior to analysis to not lead to an underestimation of wave height.

To account for the dynamic pressure loss at the sensor depth, the recorded pressure data were split into hydrostatic and dynamic pressure signals. The dynamic pressure data was corrected using a pressure response factor based on linear wave theory. The hydrostatic pressure was calculated by taking the mean over each hourly burst. The dynamic pressure was then calculated by de-trending the pressure signal, by subtracting the hydrostatic pressure, i.e. the mean water depth, from the pressure signal. The mean pressure in each burst is the hydrostatic pressure, and the remaining values after the mean is subtracted from data in that burst is the dynamic pressure. The original water surface elevation (η), which is accounting for dynamic pressure loss, is calculated as:

$$p = -\rho g z + \rho g \frac{H}{2} \cos(kz - \sigma t) \frac{\cosh(k(h+z))}{\cosh kh} = -\rho g z + \rho g \eta K_p(z)$$

$$K_p(z) = \frac{\cosh(k(h+z))}{\cosh kh}$$

In the above, p is the toral pressure recorded by the pressure sensor, $-\rho g z$ is the static pressure (ρ is water density, g is acceleration due to gravity and z is the depth of the pressure sensor). $\rho g H K_p(z)/2$ is the dynamic pressure (H is the wave height and K_p is the pressure response factor. k is calculated by: $k = 2\pi/L$, where L is the wavelength. Calculation of the wavelength requires the solution of the wave dispersion equation for the specific depth, knowing the wave period through Fourier transforms.

In this study, a Matlab toolbox (Karimpour and Chen, 2017), OCEANLYZ (Ocean Wave Analyzing Toolbox), for analyzing the wave time series data collected by pressure sensors was used for data analysis. This toolbox provides options for both frequency (spectral) and time domain (zero-crossing wave) analysis. The toolbox was used to calculate wave properties such as wave height and wave period in the frequency domain. The toolbox was also used to correct and account for the pressure attenuation (pressure loss) in the water column for data collected by the pressure sensors. All of the pressure sensors were located ~2 m below the water surface in water depth of ~10 m. Therefore, the pressure attenuation factor was relatively small.

The main wave parameters for both wind/swell waves and infragravity waves are defined in Table 2. The definition and the integration interval for IG waves in an example spectrum are shown on Figure 15.

To resolve the finer scale wave energy in the IG band, additional integration was undertaken in the following wave period bands: 30-50 s; 50-60 s; 60-70 s; 70-90 s; 90-100 s; 100-120 s; 120-130 s; 130-150 s; 150-200 s. These bands correspond to $f_{lower,IG}$ - $f_{upper,IG}$ in the moment calculations defined in Table 2.

The groupiness of ocean waves has been related to infragravity waves with a parameter 'groupiness factor (GF)' that was defined by List (1991) to assess the degree of groupiness in a wave time series. GF ranges between 0 and 1 with GF=1 showing a 'perfect' groupiness where the maximum wave height in the envelope is double the incident wave height and the minimum wave height in the envelope is zero (see Figure 3).

Table 2. Definition of wave parameters

Parameter	Equation	Comments
Significant wave height (m)	$H_s = 4\sqrt{m_0}$	m_0 is the zeroth moment
Modal wave height (s)	$T_m = \sqrt{m_0/m_2}$	m_0 is the zeroth moment
Moment definition	$m_n = \int_{f_{lower}}^{f_{upper}} f^n \, E(f) \, df$	Definition n^{th} of moment. f is frequency, E(f) is spectral energy. For swell waves f_{lower} and f_{upper} were 8 and 25 s, respectively
IG wave height (m)	$H_{s,IG} = 4\sqrt{m_{0,IG}}$	$m_{0,IG}$ is the zeroth moment for IG waves
	$m_{n,IG} = \int_{f_{lower,IG}}^{f_{upper,IG}} f^n \, E(f) \, df$	Definition n^{th} of moment. f is frequency, E(f) is spectral energy. For IG waves $f_{lower,IG}$ and $f_{upper,IG}$ were 30 and 200 s respectively

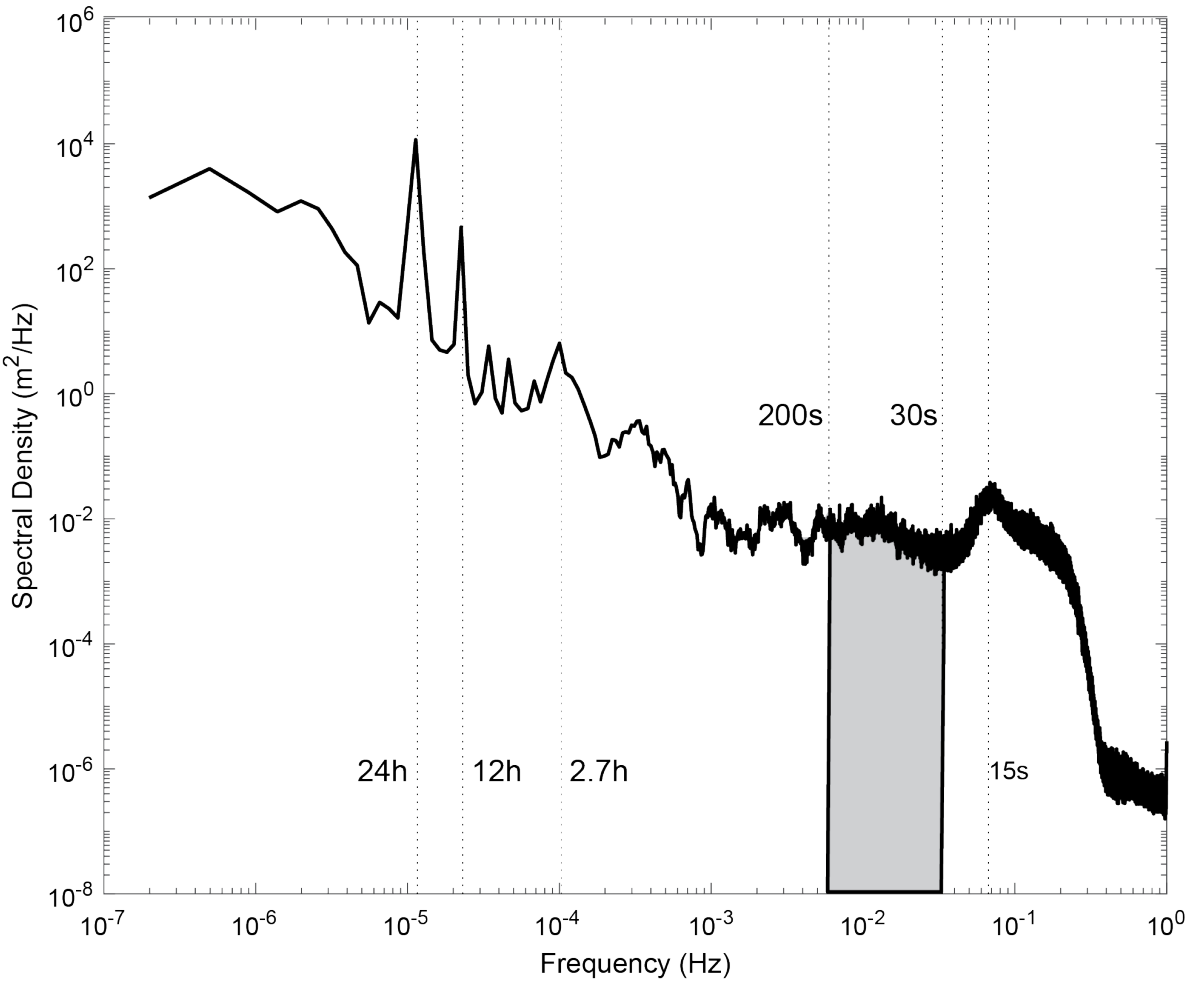

Figure 15. Definition of the infragravity wave band (30-200 s) in the water level spectrum.

4 Results

4.1 Water level spectra

4.1.1 Seasonal changes

The general pattern of monthly water level spectra show similar patterns at the Stirling Channel station in 2022 (Figure 16). In the longer periods, there are spectral energy peaks at 12 and 24 hours indicating the tidal forcing with the highest spectral energy (Figure 16, also Figures 8 and 9). There is another peak at 2.7 hours that represents the continental shelf seiche which is a common feature in this region and due to the oscillation on the continental shelf (Figures 8, 9, 16). In the swell band, the main peak is at 15 s that is consistent throughout the year (Figure 16). These spectral peaks were the only peaks that were higher than the 95% confidence interval (shown in the spectrum for June, Figure 16).

There was a decrease in spectral energy at the peak period of 15 s with a minimum (spectral valley) at 30 s and then an increase in energy to the ~100 s period and then a decrease to 200 s (Figure 16). The peak period at ~100 s was not present in December with the spectral energy increasing almost linearly from 30 to 200 s.

4.1.2 Time-frequency spectra

The Stirling Channel monthly time frequency water level spectra obtained in 2022 were similar to those recorded at other locations (Section 2.2; Figures 8, 9 and 10). The main spectral energy is concentrated in the swell band 8-15 s and the number of individual storms changes with season (Figure 17). For example, January and February 2022 had four and three storms, respectively, whilst July and August 2022 had nine and six storms, respectively. Towards the end of July 2022 (from the 20th onwards), there were several storms back-to-back. The storm in early August 2022 was the biggest (in terms of maximum wave heights offshore) experienced in the Perth region over the past 10 years. The seasonal change in the sea breeze system can also be identified for the summer months (January, February), when there is a diurnal signal in periods < 8 s (Figure 17).

In the Stirling Channel, data also reproduced the main observation in previous studies that higher spectral energy in the IG band was present when the swell wave period exceeded 15 s. This feature was present throughout the year. In summer (January/February), only a few IG events were observed but over the period July-September there were many events. Majority of these events were storm systems with observed swell > 15 s and higher spectral energy in the 8-15 s swell band and < 8 s sea band, indicating a range of wave periods and locally generated waves.

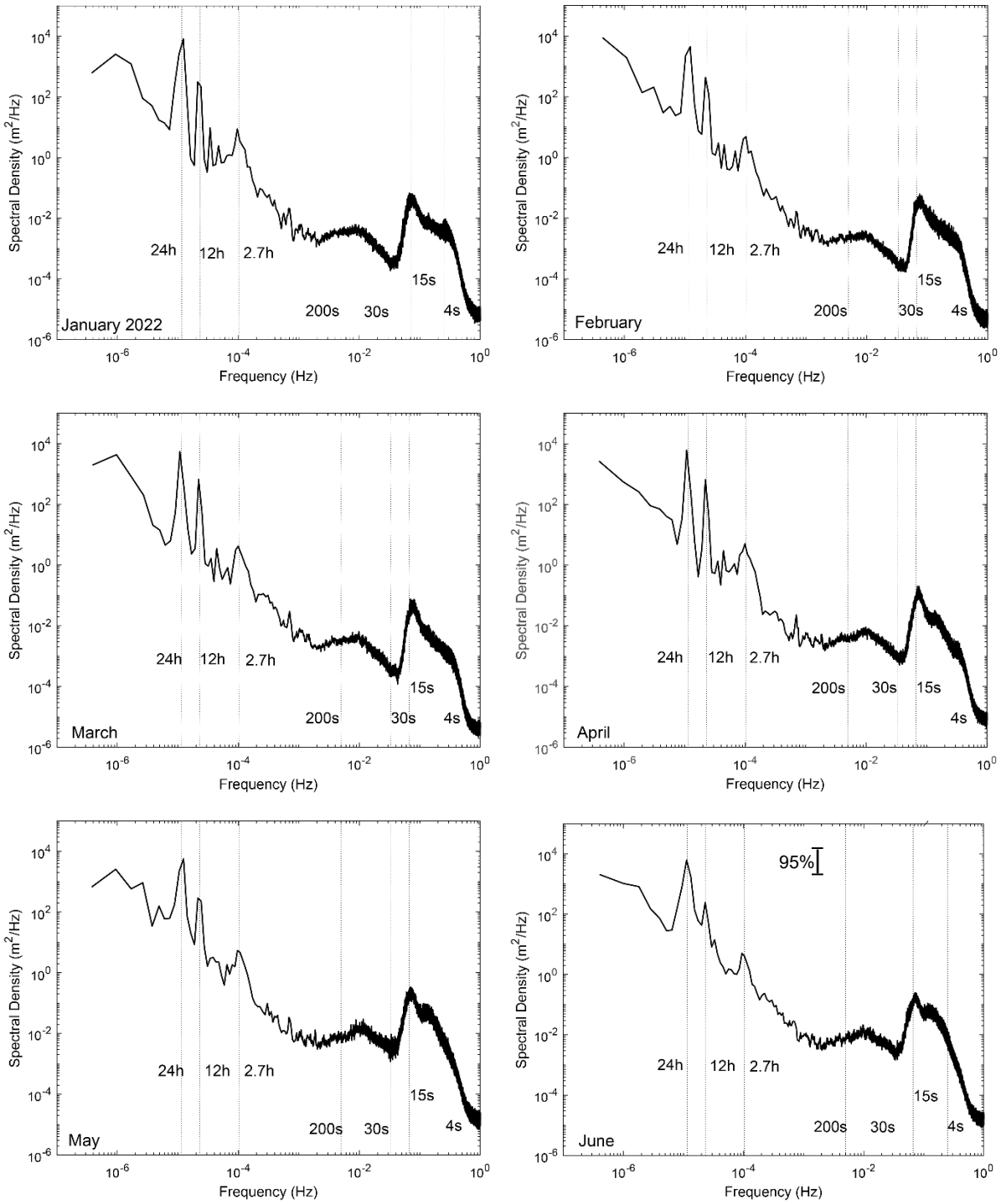

Figure 16. Monthly water level spectra at Stirling Channel in 2022 (January-June). The 95% confidence interval shown for June applies to all plots.

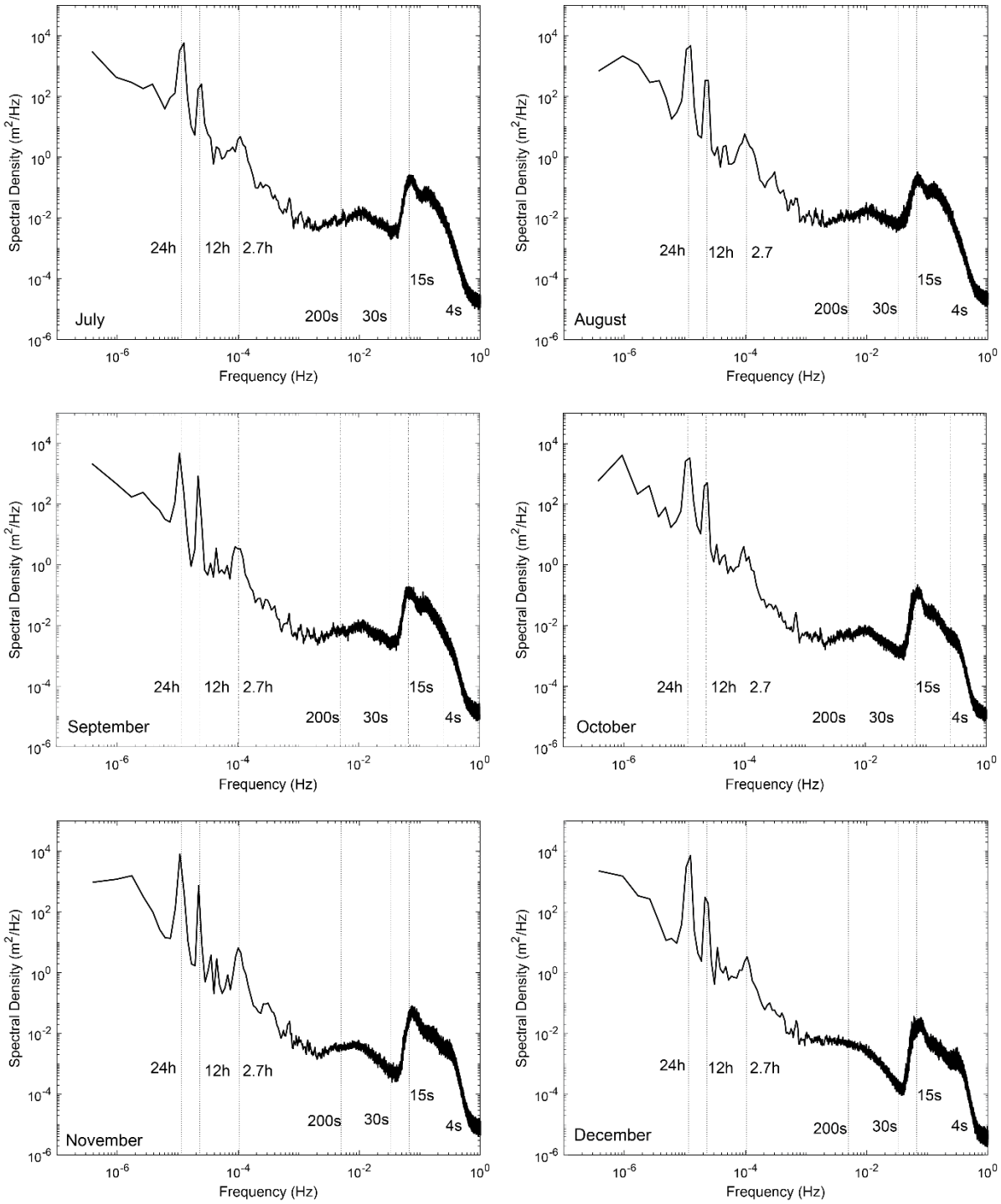

Figure 16 (cont). Monthly water level spectra at Stirling Channel in 2022 (July-December).

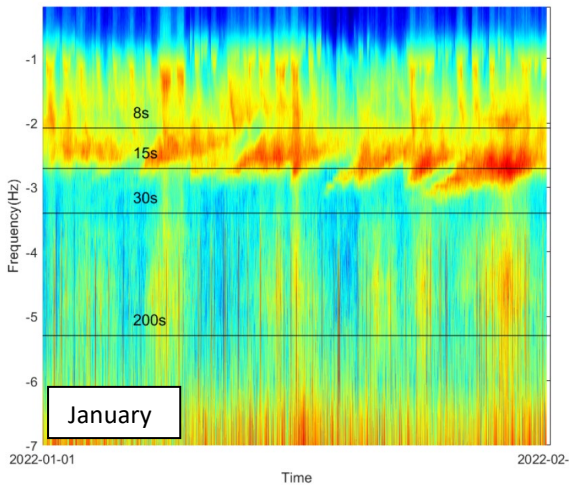
8s
15s
30s
200s
January
Frequency(Hz)
-1
-2
-3
-4
-5
-6
-7
2022-01-01
2022-02-
Time

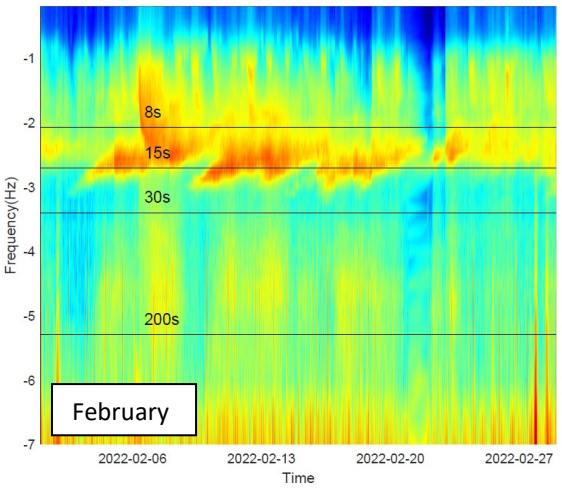
8s
15s
30s
200s
February
Frequency(Hz)
-1
-2
-3
-4
-5
-6
-7
2022-02-06
2022-02-13
2022-02-20
2022-02-27
Time

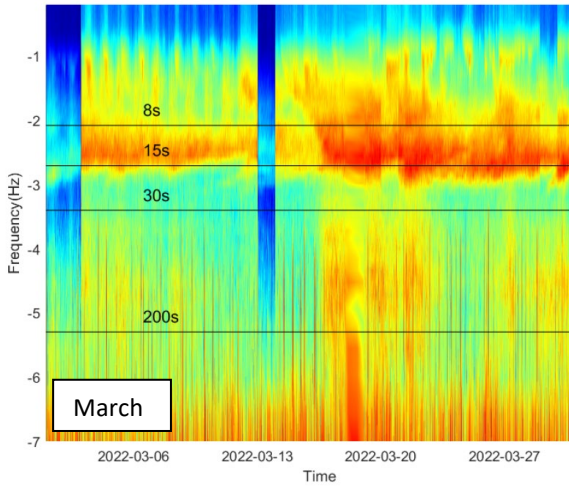
8s
15s
30s
200s
March
Frequency(Hz)
-1
-2
-3
-4
-5
-6
-7
2022-03-06
2022-03-13
2022-03-20
2022-03-27
Time

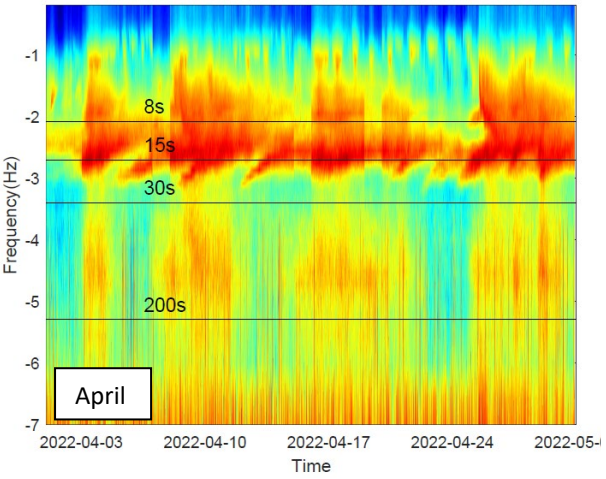
8s
15s
30s
200s
April
Frequency(Hz)
-1
-2
-3
-4
-5
-6
-7
2022-04-03
2022-04-10
2022-04-17
2022-04-24
2022-05-
Time

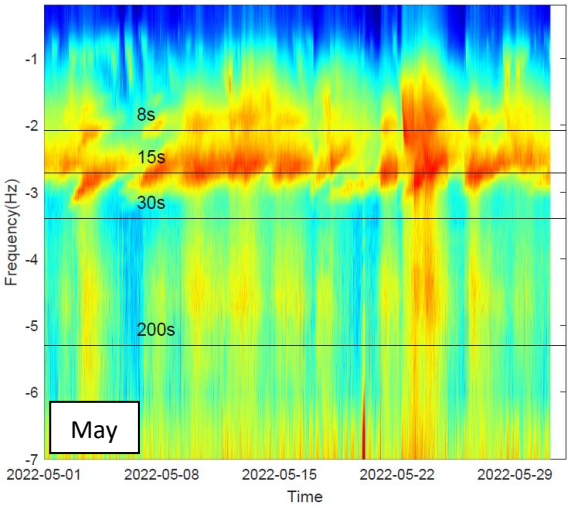
8s
15s
30s
200s
May
Frequency(Hz)
-1
-2
-3
-4
-5
-6
-7
2022-05-01
2022-05-08
2022-05-15
2022-05-22
2022-05-29
Time

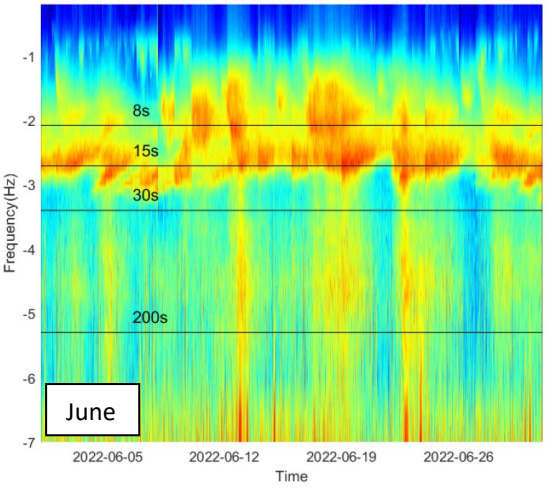
8s
15s
30s
200s
June
Frequency(Hz)
-1
-2
-3
-4
-5
-6
-7
2022-06-05
2022-06-12
2022-06-19
2022-06-26
Time

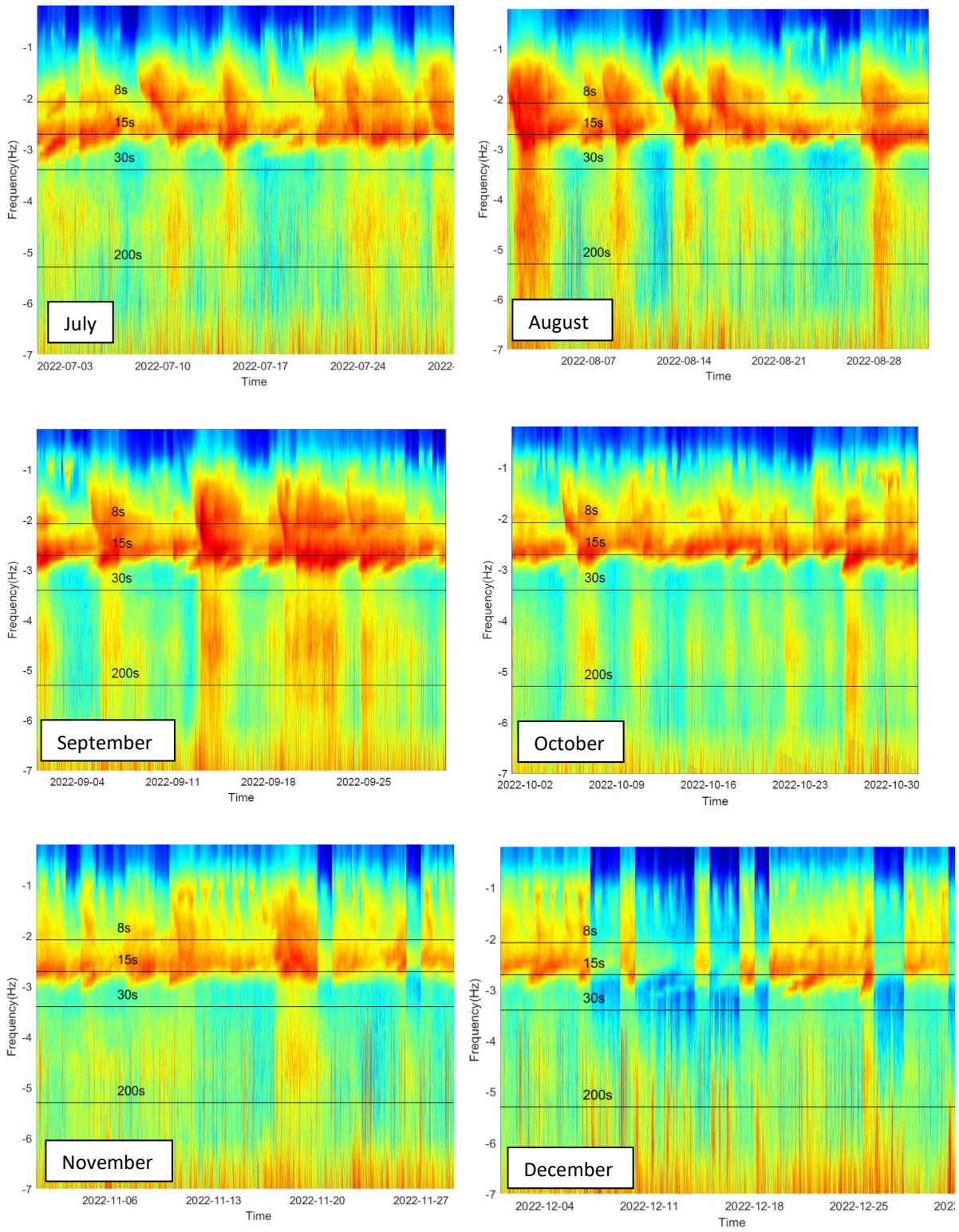

Figure 17. Monthly water level time-frequency spectra at Stirling Channel in 2022 (January-December). Note that the y-axis is a log scale.

4.1.3 Time series

Time series of significant wave height (H_s), swell and sea periods and IG wave height (H_{ig}) as defined in Table 2 are provided in Figures 18 to 21 for Stirling Channel (2020, 2022), Parmelia (2020) and Success (2022), with basic statistics of the wave parameters shown in Table 3.

Overall, Success and Parmelia recorded higher H_s and H_{ig} wave heights than Stirling Channel (Table 3). The highest H_s at Parmelia (2.2 m) was recorded in May 2020, whilst at Stirling Channel and Success, the maxima were recorded in August 2022 (1.85 and 1.97, respectively). The maximum IG wave heights at each of the sites coincided with the storm events that resulted in the highest H_s. The H_{ig} were 0.27 and 0.26 at Success (2022) and Parmelia (2020), respectively, whilst at Stirling Channel, the max H_{ig} was 0.1 m (Table 3). At Stirling Channel, the median H_s and H_{ig} were 0.18 and 0.01 m.

Table 3. Statistics of wave parameters recorded at Stirling Channel (2020, 2022), Parmelia (2020) and Success (2022)

Site	Max Hs (m)	Median Hs (m)	Std Dev Hs	Max Hig (m)	Median Hig (m)	Std Dev Hig	% Hig/Hs	50th percentile >0.05m
Stirling Channel 2020	1.85	0.18	0.01	0.1	0.01	0.01	3%	0.05
Stirling Channel 2022	1.53	0.16	0.19	0.1	0.01	0.01	3%	0.05
Success 2022	1.97	0.53	0.27	0.27	0.03	0.03	7%	0.07
Parmelia 2020	2.2	0.45	0.33	0.26	0.03	0.04	10%	0.04

The time series of H_s and H_{ig} followed a seasonal pattern with higher values observed during the winter months and lower values during summer (Figures 18-21). The same pattern was observed at all four stations. Data for 2020 (Stirling Channel and Parmelia) started on 1st May extending to 31 December but there was a gap, missing data in June-July during the peak winter months (Figures 18 and 20). For Stirling channel and Success, there was a full year of data recorded in 2022 (Figures 19 and 21). For both annual time series, the pattern was very similar, with lower H_s with a diurnal variation during the summer months due to sea breeze events and higher H_s that we associated with the passage of storm systems. The H_{ig} time series followed a similar trend with lower wave height during summer and higher during winter. There was no diurnal variation during the summer months. This is because IG waves are related to incident swell, particularly when the wave period was > 15 s (section 4.1.3).

For Stirling Channel, in 2020, the H_{ig} wave heights were constantly < 0.05 m and there were seven events where H_{ig} > 0.05 m and once > 0.1 m (Figure 18). Note that there is a lack of data during June-July which would have affected these statistics. For the full year record of 2022, a similar pattern, viz < 0.05 m for majority of the time with two events showing H_{ig} > 0.1 m and 10 events with H_{ig} between 0.05 and 0.1 m (Figure 19). In contrast, at Parmelia and Success, there were many events with H_{ig} > 0.1 m and a single event with H_{ig} > 0.25 m (Figures 20 and 21).

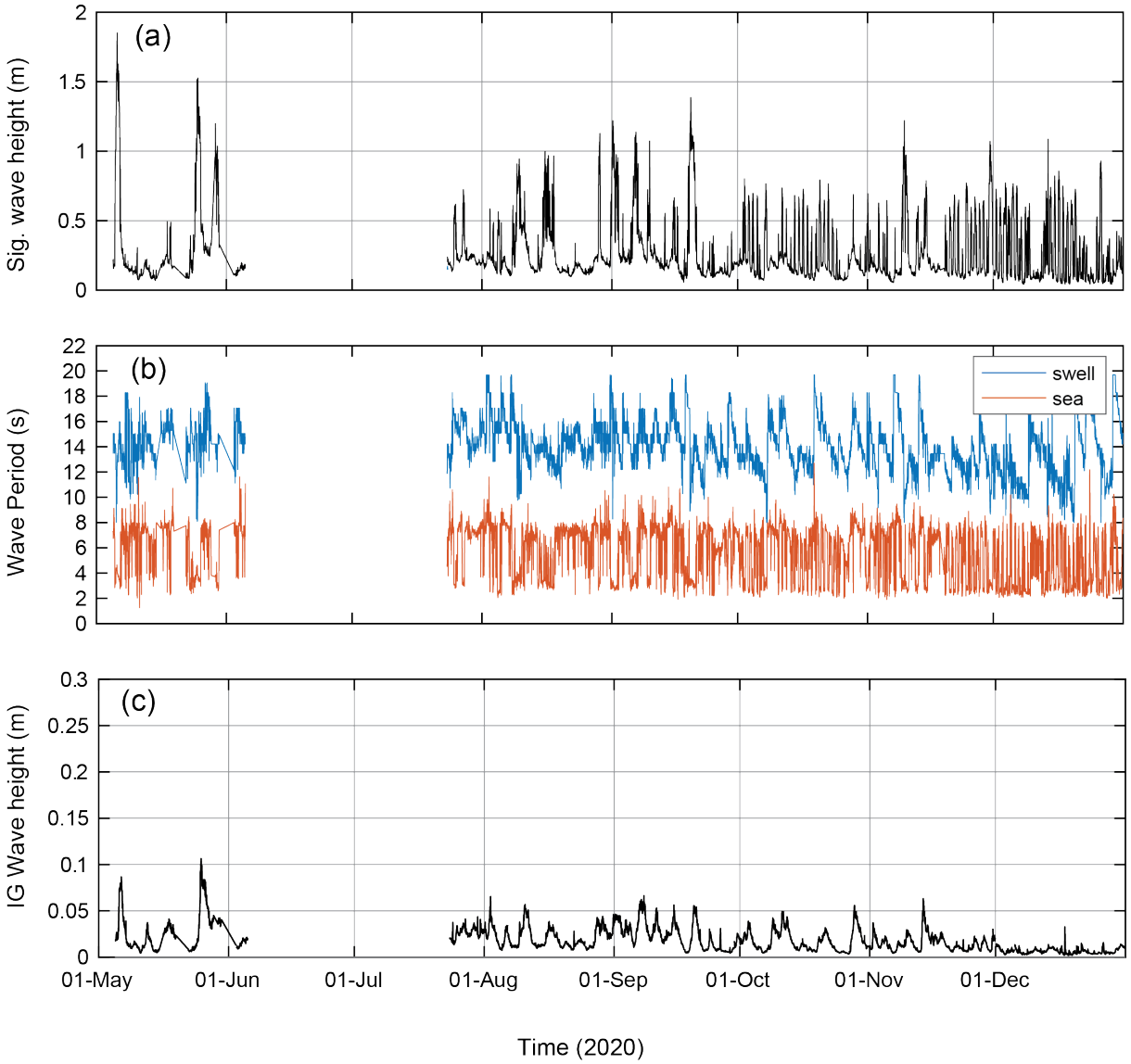

Figure 18. Annual time series of (a) significant wave height; (b) swell and sea wave period; and, (c) IG wave height at Stirling Channel in 2020.

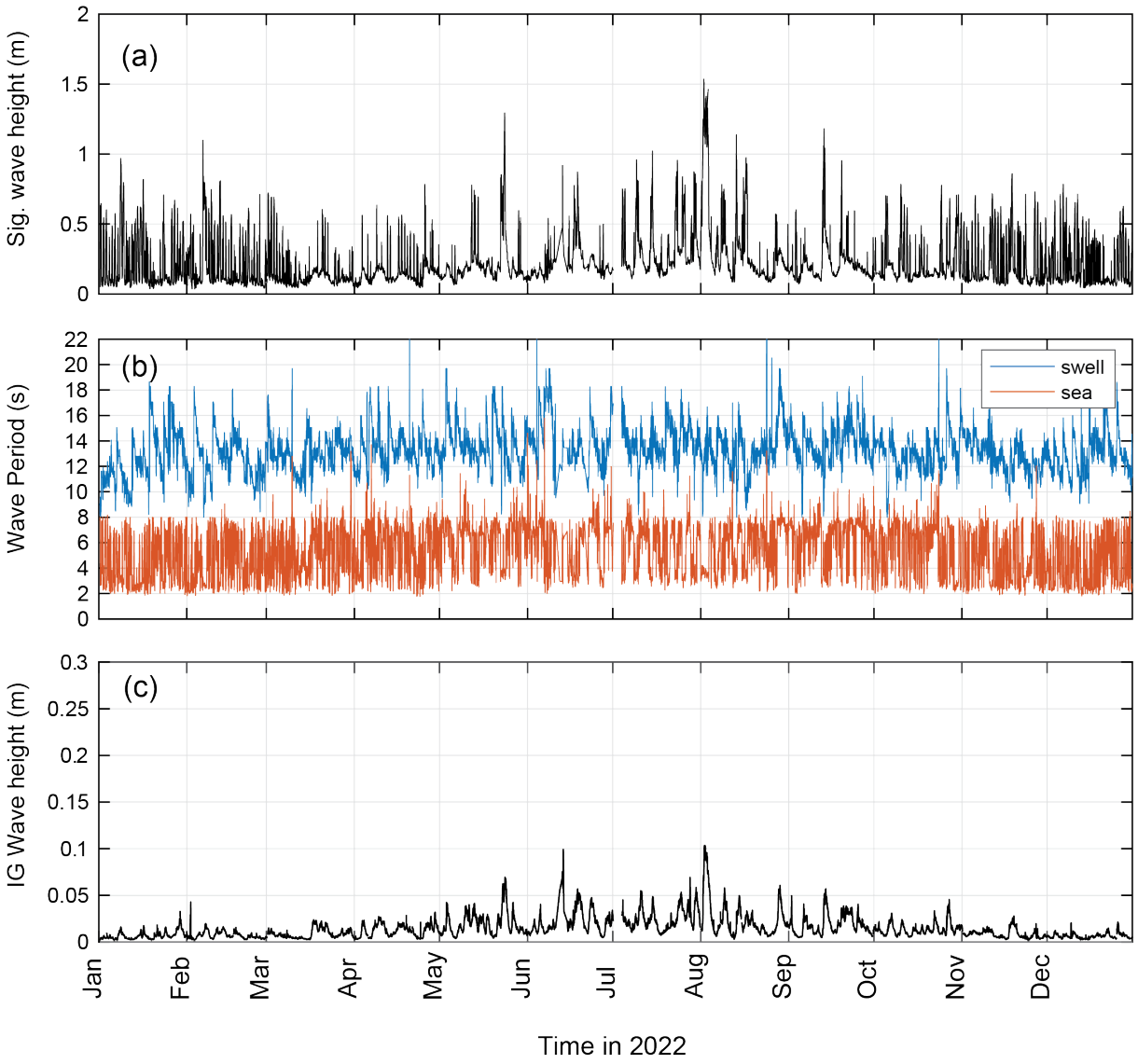

Figure 19. Annual time series of (a) significant wave height; (b) swell and sea wave period; and, (c) IG wave height at Stirling Channel in 2022.

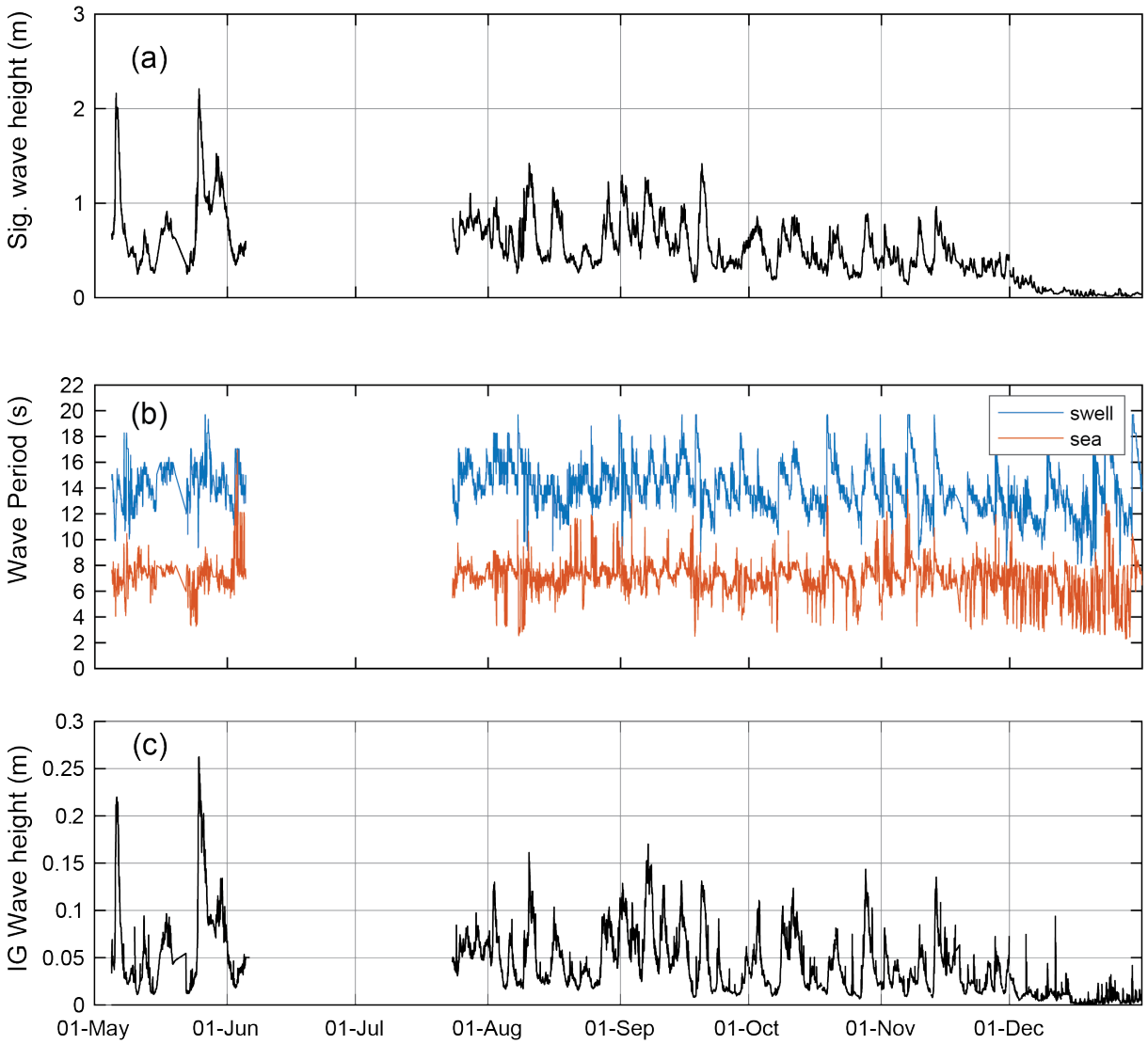

Figure 20. Annual time series of (a) significant wave height; (b) swell and sea wave period; and, (c) IG wave height at Parmelia Bank in 2020

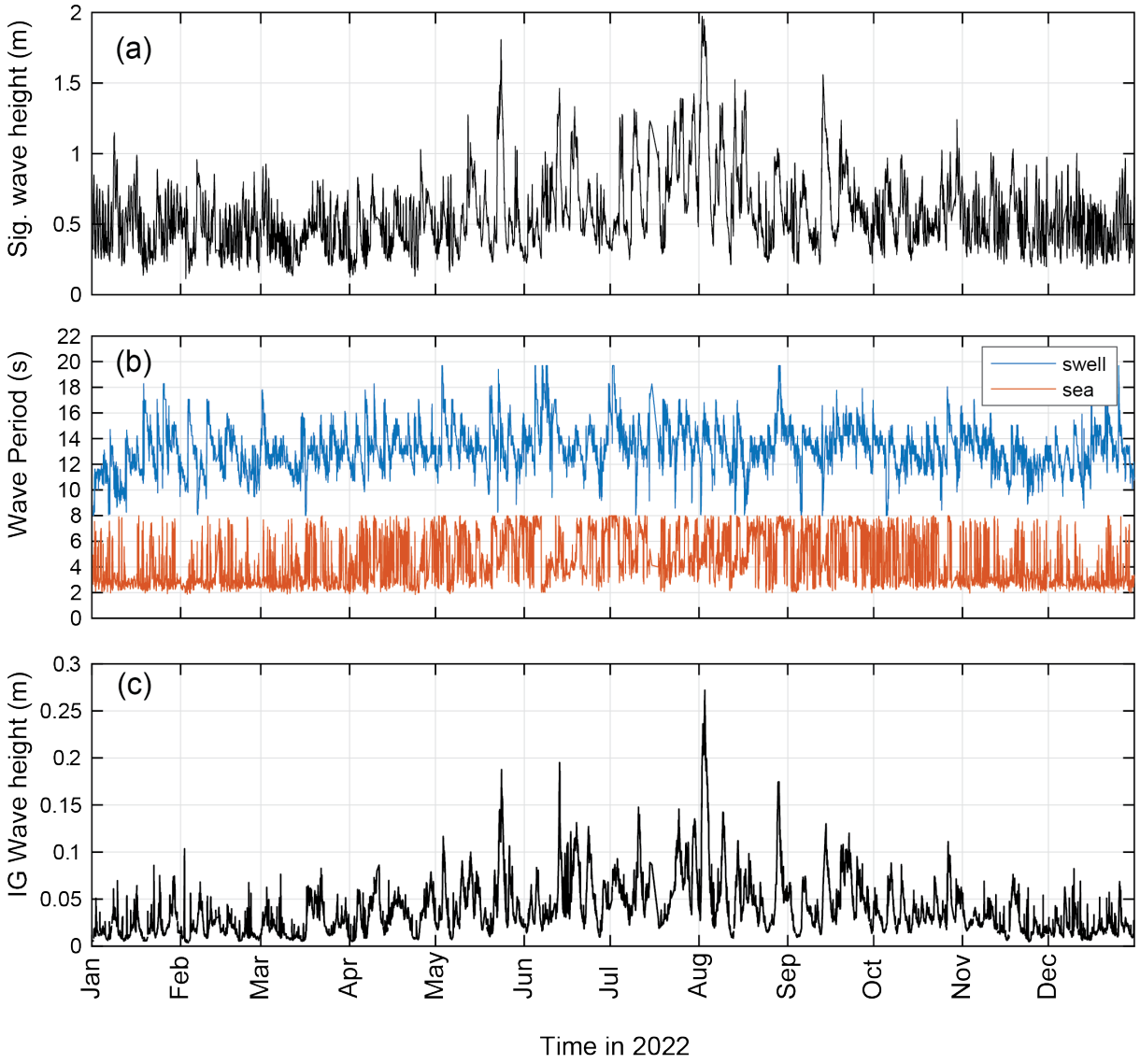

Figure 21. Annual time series of (a) significant wave height; (b) swell and sea wave period; and, (c) IG wave height at Success Bank in 2022.

4.1.4 Distribution of significant and infragravity wave heights

The histograms of H_s for data in 2020 are compromised given that data were not available for the complete year as well as for a significant period over winter (Figure 22). Comparison between Stirling Channel and Success in 2022 shows that the distribution at Success was such that the higher waves were present compared to Stirling Channel (Figure 22 b, d). Wave statistics for each station are listed in Table 3. It should be noted that a significant percentage of H_s at Stirling Channel was < 0.25 m (Figure 22b).

The H_{ig} distributions indicated a high percentage of H_{ig} < 0.05 m at Stirling Channel in 2022 (Figure 23b), whilst a higher percentage of H_{ig} occurrence was recorded at Success in 2022 (Figure 23d).

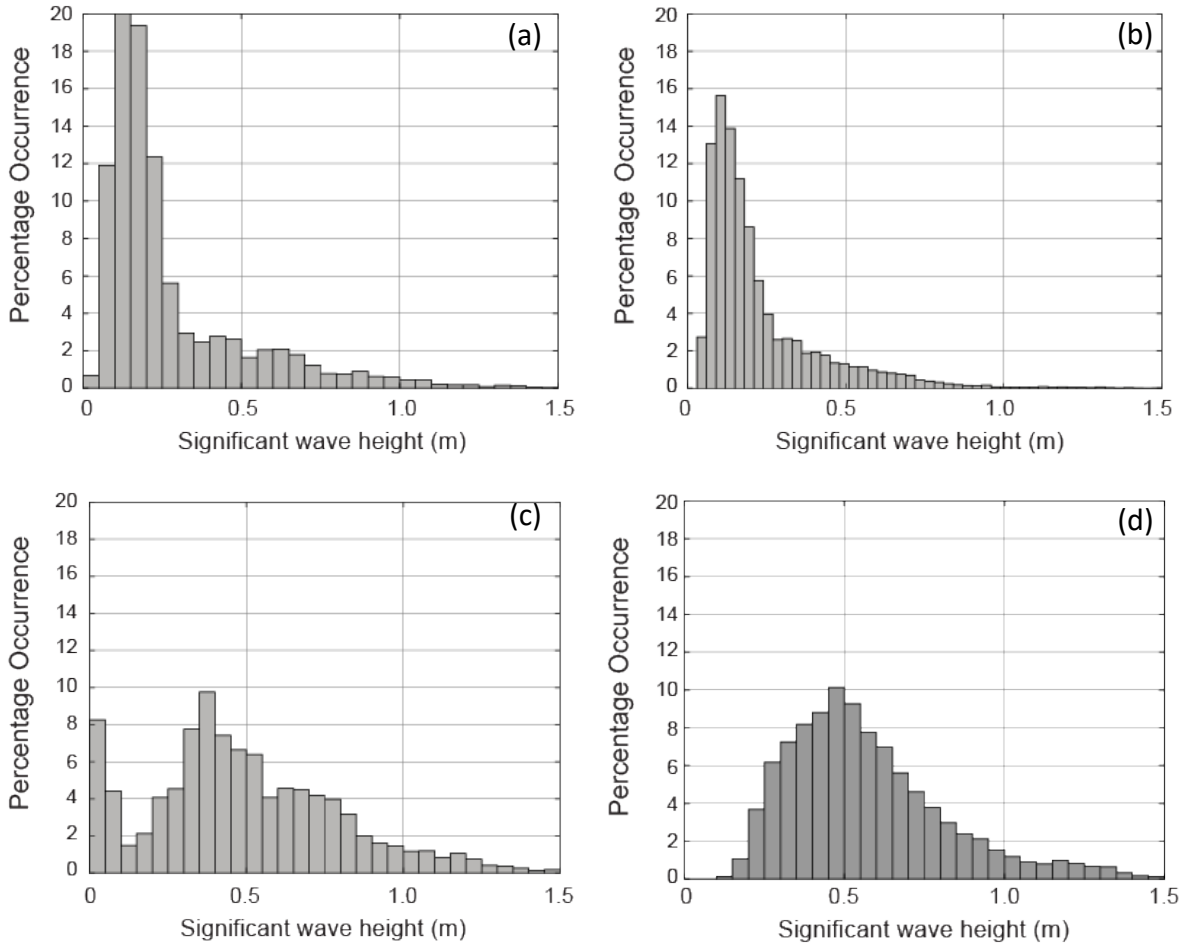

Figure 22. Distribution of significant wave heights for (a) Stirling Channel 2020; (b) Stirling Channel 2022; (c) Parmelia 2020; and, (d) Success in 2022.

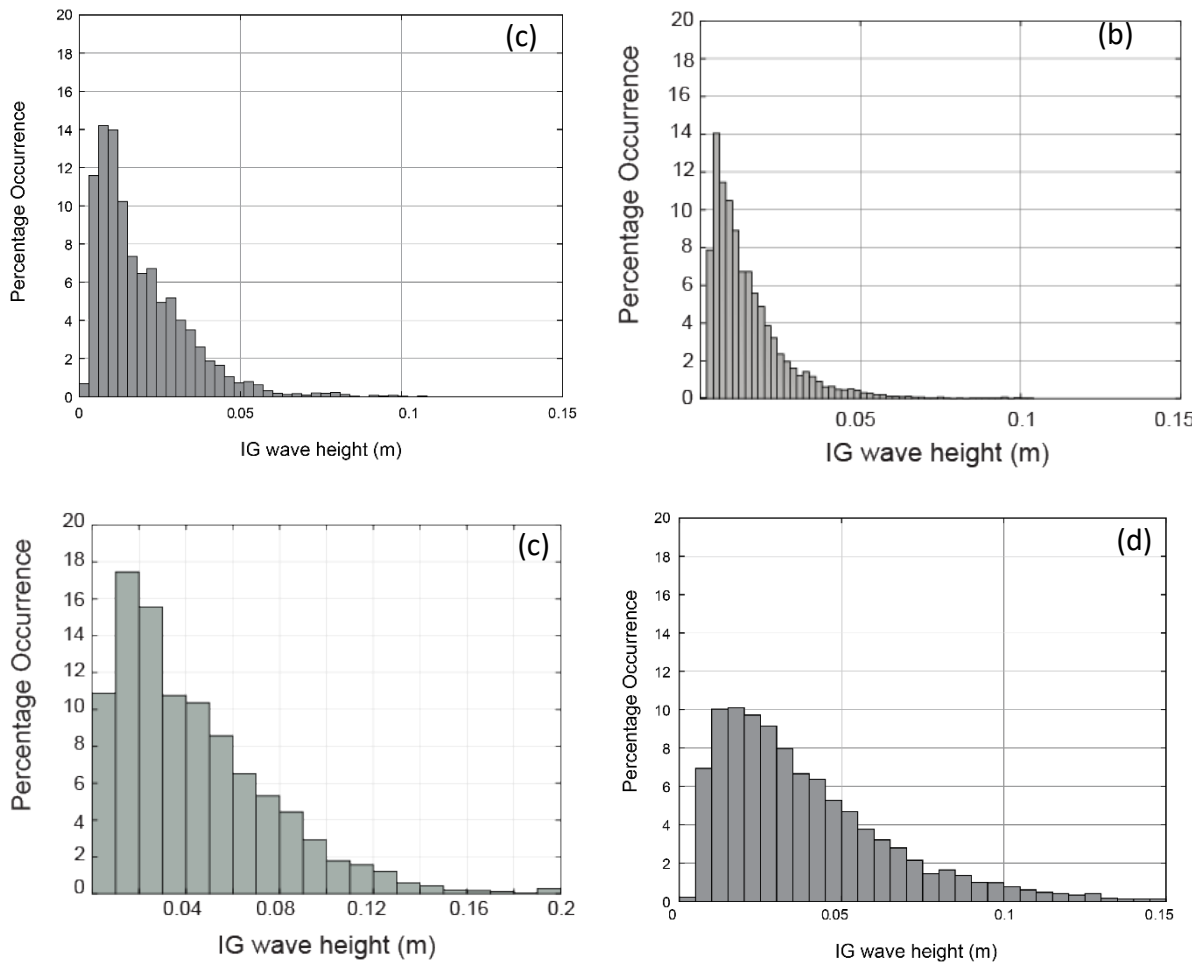

Figure 23. Distribution of infragravity wave heights for (a) Stirling Channel 2020; (b) Stirling Channel 2022; (c) Parmelia 2020; and, (d) Success 2022.

4.1.5 Relationship between significant and infragravity wave heights

The time-frequency water level spectra indicated that IG energy was generally present when the incident wave periods were > 15 s (Section 4.1.2). Similarly, historical data indicated a linear relationship between H_s and H_{ig} (Figure 11). Scatter plots between H_s and H_{ig} did not indicate a strong linear relationship, although, there was a trend for increasing H_s related to increasing H_{ig} at all the stations (Figure 24). At Stirling Channel, both 2020 and 2022 data indicated two separate linear relationship between H_s and H_{ig} (Figures 24a, b).

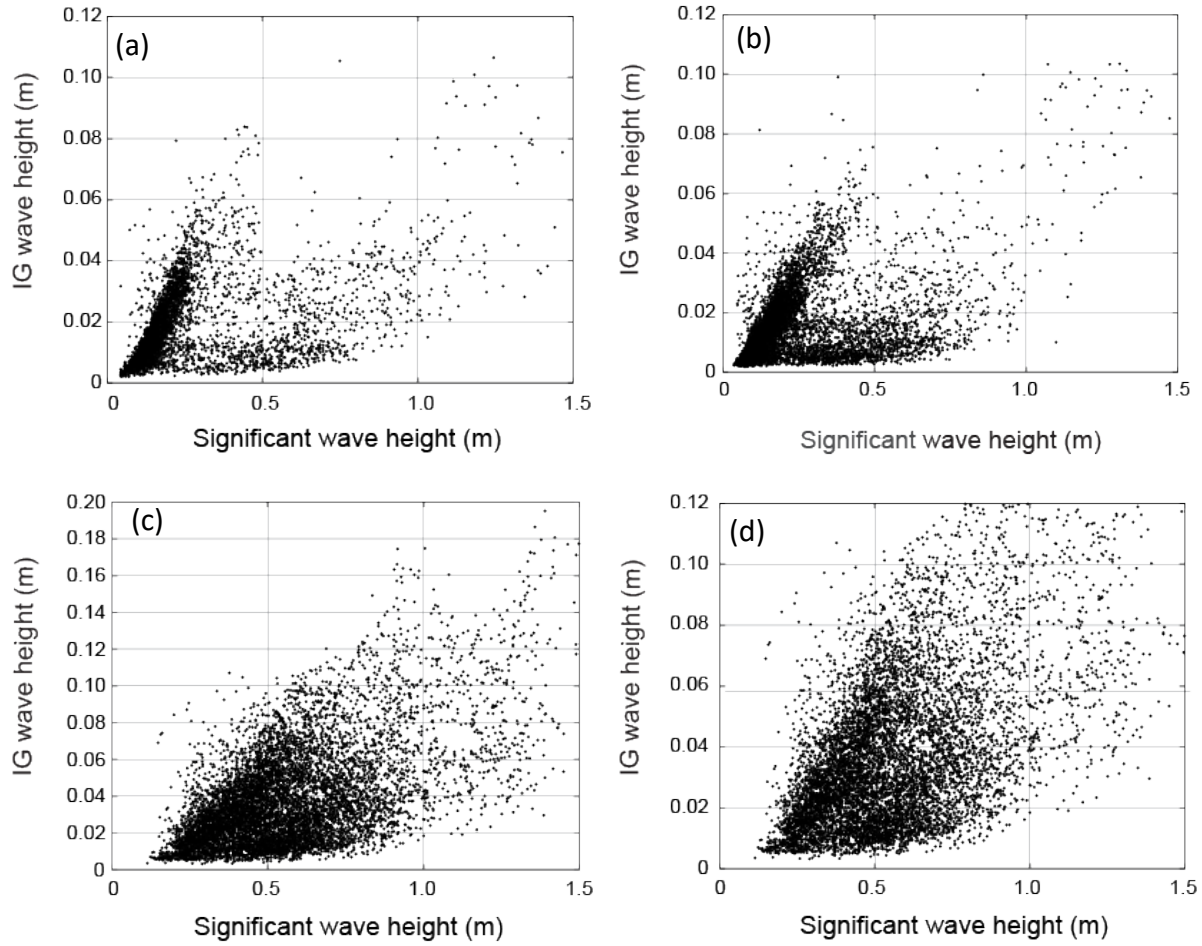

Figure 24. Scatter plots of significant and infragravity wave heights for (a) Stirling Channel 2020; (b) Stirling Channel 2022; (c) Parmelia 2020; and, (d) Success 2022.

4.1.6 Infragravity waves in different period bands

In this report, we define the infragravity waves as an integration of spectral energy in the period of 30-200 s (Table 2). It is also possible to narrow the period bands corresponding to $f_{lower,IG}$ and $f_{upper,IG}$ in the moment calculations defined in Table 2. To resolve the finer scale wave energy in the IG band, additional integration was undertaken in the following wave period bands: 30-50 s; 50-60 s; 60-70 s; 70-90 s; 90-100 s; 100-120 s; 120-130 s; 130-150 s; 150-200 s. The spectral plots did not indicate any significant peaks in the 30-200 s band and, therefore, it is unlikely to identify specific recurring periods with higher wave height.

The analysis was applied to the Stirling Channel data in 2022 and four months were selected for analysis: March, June, July and August (Figures 25-28). The latter months include energetic storms whilst March is a relatively low period for swell events.

The groupiness factor (GF) was also calculated for each month and the results showed that GF fluctuated around 0.5 (Figures 25-28), indicating a moderate amount of groupiness in the incoming swell (List, 1991).

In March 2022, the H_s was < 0.8 m with the higher values associated with sea breeze at the beginning of the month (Figure 25a). H_{IG} was consistently low, < 0.02 m, with some isolated events that reached 0.05 m. (Figures 25d-g).

In the winter months (June, July, August, 2022), H_s was up to 1.0 m (in August it was > 1.5 m associated with a major storm) but the H_{IG} waves were still < 0.05 m (Figures 26-28).

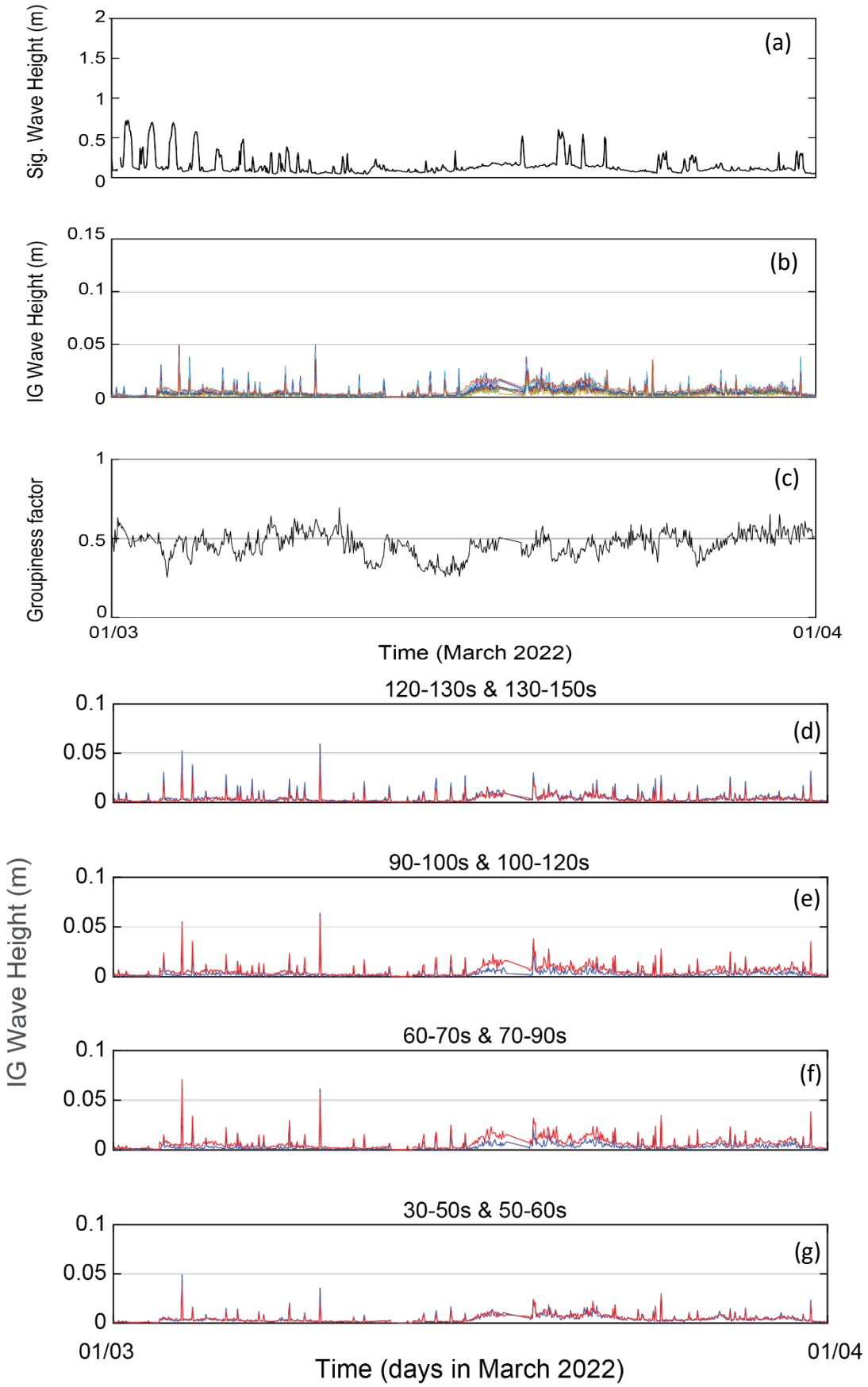

Figure 25. Time series of (a) significant wave height; (b) infragravity wave heights at specific periods 30-50 s; 50-60 s; 60-70 s; 70-90 s; 90-100 s; 100-120 s; 120-130 s; 130-150 s; 150-200 s; (c) groupiness factor; (d-g) infragravity wave heights at different periods. Stirling Channel, March 2022.

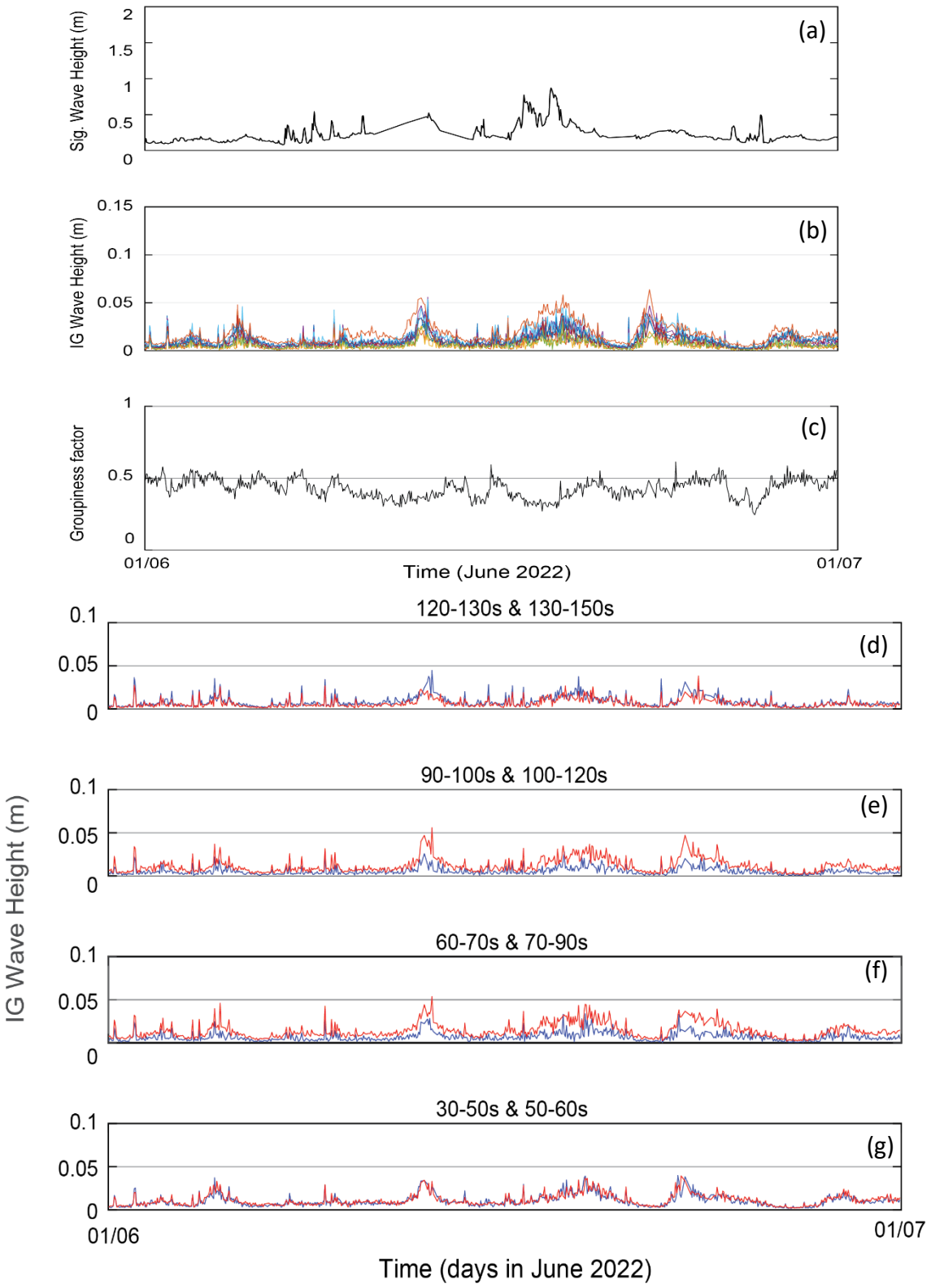

Figure 26. Time series of (a) significant wave height; (b) infragravity wave heights at specific periods 30-50 s; 50-60 s; 60-70 s; 70-90 s; 90-100 s; 100-120 s; 120-130 s; 130-150 s; 150-200 s; (c) groupiness factor; (d-g) infragravity wave heights at different periods. Stirling Channel, June 2022.

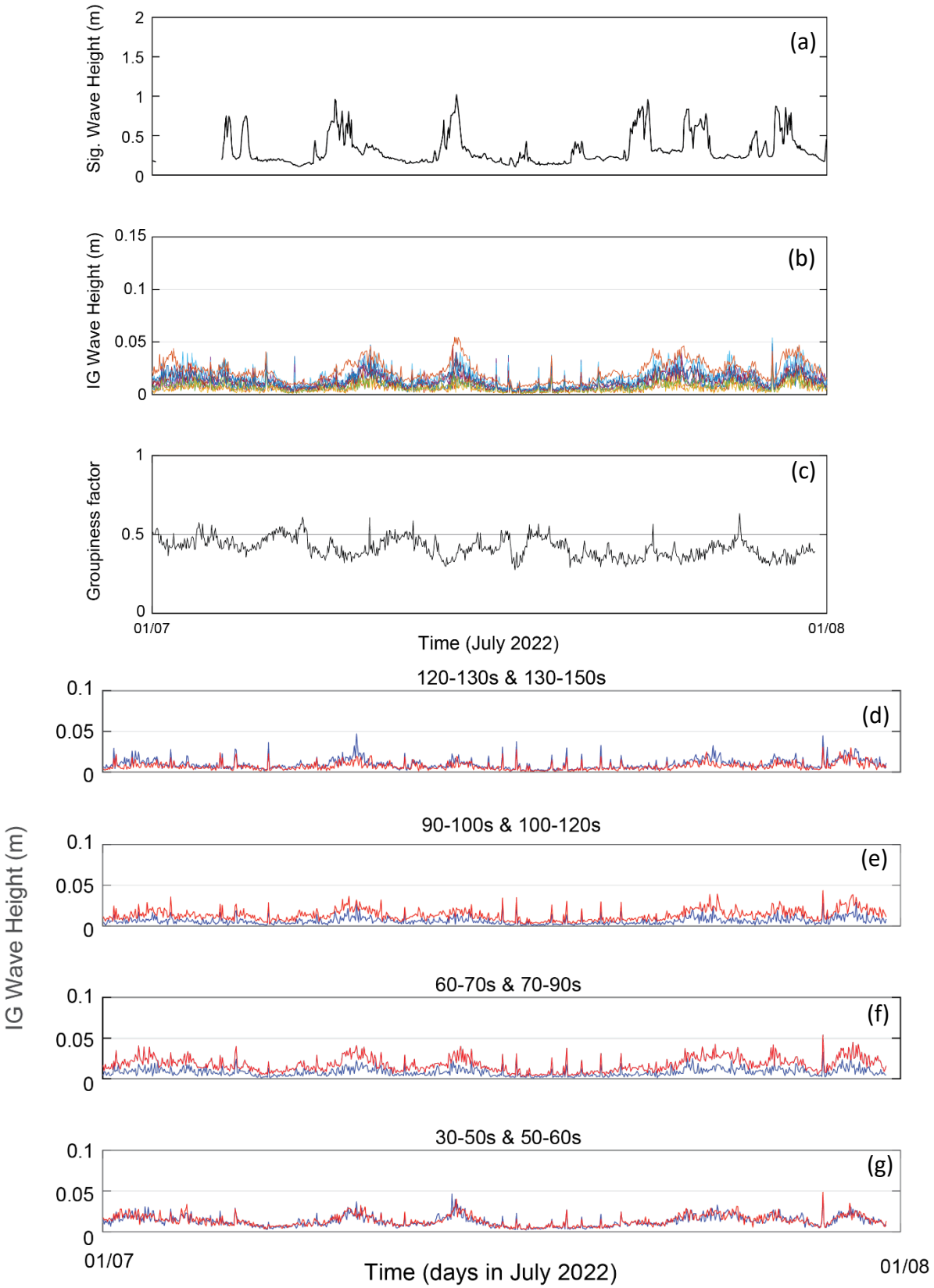

Figure 27. Time series of (a) significant wave height; (b) infragravity wave heights at specific periods 30-50 s; 50-60 s; 60-70 s; 70-90 s; 90-100 s; 100-120 s; 120-130 s; 130-150 s; 150-200 s; (c) groupiness factor; (d-g) infragravity wave heights at different periods. Stirling Channel, July 2022.

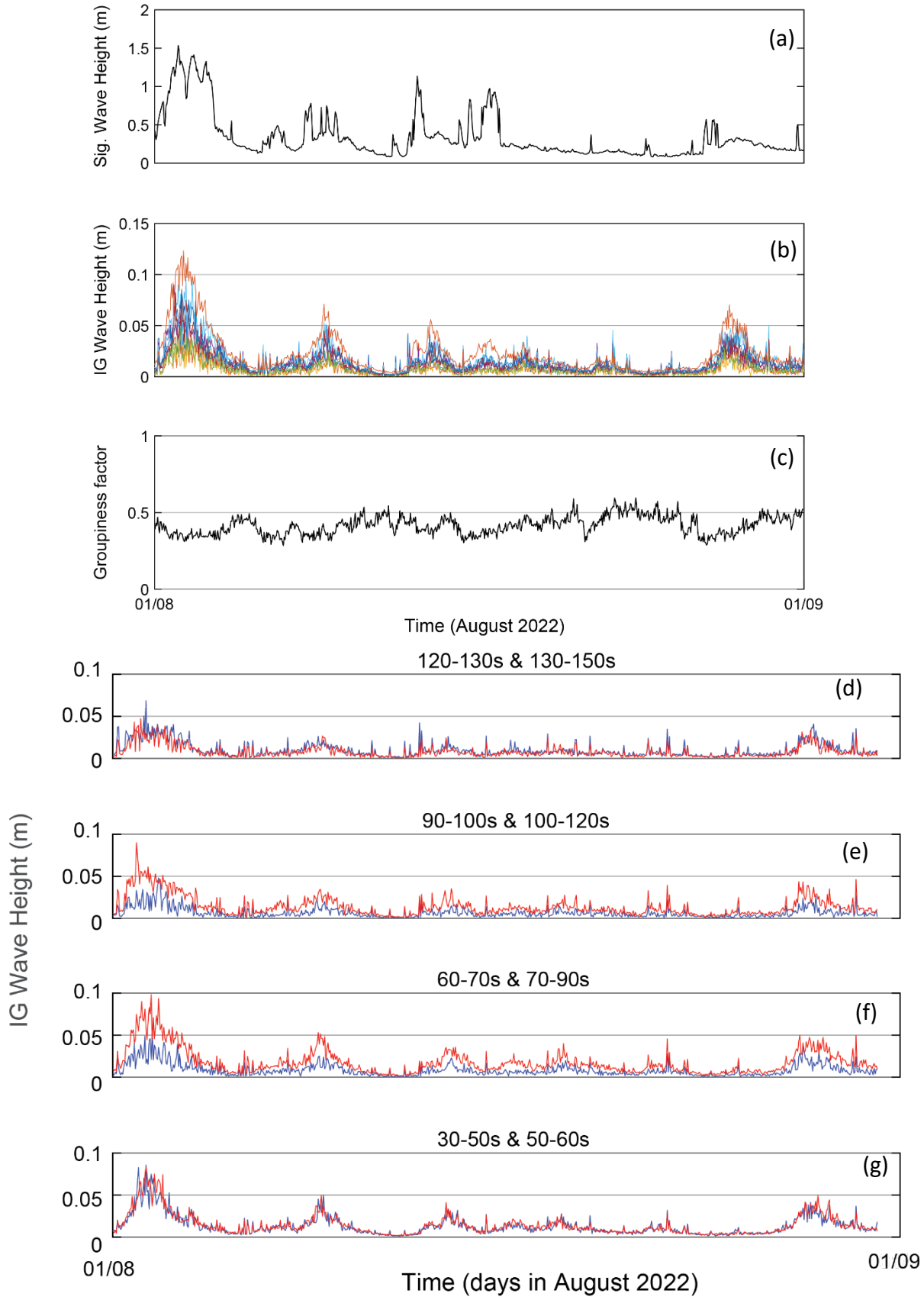

Figure 28. Time series of (a) significant wave height; (b) infragravity wave heights at specific periods 30-50 s; 50-60 s; 60-70 s; 70-90 s; 90-100 s; 100-120 s; 120-130 s; 130-150 s; 150-200 s; (c) groupiness factor; (d-g) infragravity wave heights at different periods. Stirling Channel, July 2022.

5 Discussion / Conclusions

Surface gravity waves incident on a coastal region can be classified into three main groups depending on their period: (1) sea waves, generated by local weather, with periods between 2 and 8s; (2) swell waves, generated by distant storms, with periods between 8 and 25s; and (3) infragravity waves, with periods between 30 and 300s. Infragravity waves are due to the formation of wave groups, or "sets." When wind-waves of similar periods travel together, they group, resulting in varying wave heights within the groups (Figures 3,4). This wave height variation at the group scale forces infragravity waves. Coastal circulation, flooding, sand transport, and erosion are strongly influenced by these infragravity waves, especially during storms events. They also have a large influence on forcing oscillations in marinas and ports that influence vessel motion. Infragravity waves have been reported as one of the causes of oscillation problems in many ports and harbours. In a port with lengths of the order of 500 m and depths of the order of 10 m, the natural oscillation periods are of the order of a few minutes and coincide with the infragravity waves with typical periods of 30 to 300 s. When the periods of incident infragravity waves approach natural oscillation period or periods of a port, strong oscillations in the harbour basin can be generated in the infragravity band, through resonance. This results in water level fluctuations and strong horizontal currents within the port. In such conditions, if the port oscillation periods coincide with natural period of moored vessels, port operations can be interrupted due to undesirable vessel movements. This situation further causes damage to mooring lines and fenders, resulting in port downtimes followed by significant economic losses. Hence, the aim of this project was to complete an assessment of infragravity period wave activity in Cockburn Sound, particularly along the Stirling Channel, using existing field measurements. In this report, we define 'infragravity waves' or IG waves as those with periods between 30 s and 200 s that are important for vessel movements.

We analysed a unique data set that included continuous sampling of water levels at 2Hz intervals from three locations and two separate years: Stirling Channel (2020, 2022), Parmelia and Success (Figure 13). The data were analysed using a dedicated MATLAB toolbox OCEANLYZ (Karimpour and Chen, 2017) in the frequency domain.

The main outcomes of the study are as follows:

(1) Water level spectra at each of the location and throughout the year did not indicate specific periods in the 30-200 s band, rather the spectral energy was distributed almost uniformly across the IG periods. There were no peaks higher than the 95% confidence interval.
(2) The time-frequency water level spectra indicated increased energy in the 30-200 s band when the incoming swell was > 15 s. This is typical for this region of the coast.
(3) In Stirling Channel, the H_{IG} was generally low with maximum values of 0.10 m achieved during storm events.
(4) There was no clear relationship between H_s and H_{IG} although in general higher H_{IG} were associated with higher H_s.

It is concluded that the infragravity wave activity is relatively low in Cockburn Sound and in particular in the Stirling Channel. Higher H_{IG} were mainly associated with storm systems, particularly during winter when the incoming swell period was > 15 s.

6 References

Ardhuin, F., Rawat, A., & Aucan, J. (2014). A numerical model for free infragravity waves: definition and validation at regional and global scales. Ocean Modelling, 77, 20–32.

Beetham, E. P., & Kench, P. S. (2011). Field observations of infragravity waves and their behaviour on rock shore platforms. Earth Surface Process and Landforms, 36, 1872-1888.

Bertin, X., de Bakker, A., Van Dongeren, A., Coco, G., Gael, A., Ardhuin, F., Bonneton, P., Bouchette, F., Castelle, B., Crawford, W., Davidson, M., Deen, M., Dodet, G., Guerin, T., Inch, K., Leckler, F., McCall, R., Muller, H., Olabarrieta, M., Roelvink, D. (2018). Infragravity waves: from driving mechanisms to impacts. Earth-Science Reviews, 177, 774–799.

Bowen, A. J., & Huntley, D. A. (1984). Waves, long waves and nearshore morphology. Marine Geology, 60(1-4), 1-13.

Bowers, E. C. (1977). Harbour resonance due to set-down beneath wave groups. Journal of Fluid Mechanics, 79(1), 71-92.

Elgar, S., Herbers, T. H. C., Okihiro, M., Oltman-Shay, J., & Guza, R. T. (1992). Observations of infragravity waves. Journal of Geophysical Research-Oceans, 97(C10), 15,573-515,577.

Gallagher, B. (1971). Generation of surf beat by non-linear wave interactions. Journal of Fluid Mechanics, 49(1), 1-20.

Giese, G. S., & Chapman, D. C. (1993). Coastal Seiches. Oceanus, Spring, 38-45.

Herbers, T. H. C., Elgar, S., & Guza, R. T. (1994). Infragravity-frequency (0.005-0.05 Hz) motions on the shelf. Part I: forced waves. Journal of Physical Oceanography, 24(5), 917-927.

Herbers, T. H. C., Elgar, S., & Guza, R. T. (1995). Generation and propagation of infragravity waves. Journal of Geophysical Research-Oceans, 100(C12), 24,863-824,872.

Herbers, T. H. C., Elgar, S., Guza, R. T., & O'Reilly, W. C. (1995). Infragravity-frequency (0.005-0.05 Hz) motions on the shelf. Part II: free waves. Journal of Physical Oceanography, 25, 1063-1079.

Huntley, D. A. (1976). Long-period waves on a natural beach. Journal of Geophysical Research, 81(36), 6441-6449.

Janssen, T. T., Battjes, J. A., & van Dongeren, A. R. (2003). Long waves induced by short-wave groups over a sloping bottom. Journal of Geophysical Research-Oceans, 108(C8), 1-13. doi: 10.1029/2002JC001515.

Karimpour A. and Chen Q. (2017). Wind wave analysis in depth limited water using OCEAANLYZ, a MATLAB toolbox Computers and Geosciences, 106, 181-189

Kinsman, B. (1965). Wind waves: their generation and propagation on the ocean surface. Englewood Cliffs, New Jersey: Prentice-Hall, Inc.

Kularatne SR & Pattiaratchi CB. (2014). The role of infragravity waves in near-bed cross-shore sediment flux in the breaker zone. Journal of Marine Science and Engineering, 2(3), 568–592.

List, J. H. (1992). A model for the generation of two-dimensional surf beat. Journal of Geophysical Research-Oceans, 97(C4), 5623-5635.

Liu, P. L.-F. (1989). A note on long waves induced by short-wave groups over a shelf. Journal of Fluid Mechanics, 205, 163-170.

Longuet-Higgins, M. S. (1964). Planetary waves on a rotating sphere. Proceedings of the Royal Society of London. Series A, Mathematical and Physical Sciences, 279(1379), 446-473.

Longuet-Higgins, M. S., & Stewart, R. W. (1964). Radiation stress water waves; a physical discussion with applications. Deep-Sea Research and Oceanographic Abstracts, 11(4), 529-562.

McComb, P., Johnson, D., & Beamsley, B. (2009). Numerical model study to reduce swell and long wave penetration to Port Geraldton. Proceedings of the Pacific Coasts and Ports Conference 2009. Wellington, NZ: Engineers Australia.

Munk, W. H. (1949). Surf beats. Eos, Transactions American Geophysical Union, 30(6), 849–854.

Nakamura, S., & Katoh, K. (1993). Generation of infragravity waves in breaking process of wave groups. In B. L. Edge (Ed.). Proceedings of the Twenty-third international coastal engineering conference: Coastal Engineering 1992, 990-1003. New York: American Society of Civil Engineers.

Nwogu, O., & Demirbilek, Z. (2010). Infragravity Wave motions and runup over shallow fringing reefs. Journal of Waterway, Port, Coastal, and Ocean Engineering, 136(6), 395-305.
Péquignet, A. C. N., Becker, J. M., Merrifield, M. A., & Aucan, J. (2009). Forcing of resonant modes on a fringing reef during tropical storm Man-Yi. Geophysical Research Letters, 36. (L03607).
Rabinovich, A. B. (2009). Seiches and Harbor Oscillations. In Y. C. Kim (Ed.), In Handbook of Coastal and Ocean Engineering, 193-236. Singapore: World Scientific Publishing Co. Pte. Ltd.
Ruessink, B. G. (1998). Bound and free infragravity waves in the nearshore zone under breaking and nonbreaking conditions. Journal of Geophysical Research-Oceans, 103(C6), 12,795-712,805.
Thomson, J. M. (2006). Infragravity waves over topography: generation, dissipation and reflection. Ph.D. Thesis, Massachusetts Institute of Technology and Woods Hole Oceanographic Institution.
Thotagamuwage DT & Pattiaratchi CB. (2014). Observations of infragravity period oscillations in a small marina. Ocean Engineering, 88, 435–445.
Thotagamuwage DT & Pattiaratchi CB. (2014). Influence of offshore topography on infragravity period oscillations in Two Rocks Marina, Western Australia. Coastal Engineering, 91, 220–230.
Tucker, M. J. (1950). Surf beats: Sea waves of 1 to 5 min. period. Proceedings of the Royal Society of London, 202(1071), 565-573.
Van Rijn, L. C. (1990). Principles of Fluid Flow and Surface Waves in Rivers, Estuaries, Seas and Oceans. Amsterdam: Aqua Publications.
Zou, Q. (2011). Generation, transformation, and scattering of long waves induced by a short- wave group over finite topography. Journal of Physical Oceanography, 41(10), 1842-1859.

Submitted as draft	06/06/2024
Review completed	15/08/2024
Submitted as revised draft	17/09/2024
Approved by Science Program Leadership Team	21/11/2024
Approved by WAMSI CEO	27/01/2025
Final report	

WESTERN AUSTRALIAN
MARINE SCIENCE
INSTITUTION